JGR Oceans

RESEARCH ARTICLE
10.1029/2019JC015053

Special Section:
Forum for Arctic Modeling and Observational Synthesis (FAMOS) 2: Beaufort Gyre phenomenon

# Winter Sea Ice Export From the Beaufort Sea as a Preconditioning Mechanism for Enhanced Summer Melt: A Case Study of 2016

D. G. Babb[1], J. C. Landy[2], D. G. Barber[1], and R. J. Galley[1]

[1]Centre for Earth Observation Science, University of Manitoba, Winnipeg, Manitoba, Canada, [2]Bristol Glaciology Centre, University of Bristol, Bristol, UK

**Key Points:**
- Increased ice export during winter 2016 preconditioned the region toward younger thinner ice that broke up prematurely and melted rapidly
- For the second time in the observational record, and second time in 5 years, the Beaufort Sea became ice-free during September 2016
- Winter sea ice export is significantly correlated with the regional summer sea ice minimum and represents a key preconditioning mechanism

**Supporting Information:**
- Supporting Information S1

**Correspondence to:**
D. G. Babb,
david.babb@umanitoba.ca

**Citation:**
Babb, D. G., Landy, J. C., Barber, D. G., & Galley, R. J. (2019). Winter sea ice export from the Beaufort Sea as a preconditioning mechanism for enhanced summer melt: A case study of 2016. *Journal of Geophysical Research: Oceans*, *124*, 6575–6600. https://doi.org/10.1029/2019JC015053

Received 15 FEB 2019
Accepted 8 AUG 2019
Accepted article online 13 AUG 2019
Published online 9 SEP 2019



**Abstract** During September 2016 an ice-free Beaufort Sea was observed for only the second time. Like previous regional sea ice minima (1998, 2008, and 2012), seasonal preconditioning of the ice pack toward younger, thinner ice types contributed to premature breakup that accelerated the ice-albedo feedback and enhanced summer melt. In 2016, anomalously high sea ice export and ice pack divergence during February and April promoted the unusual widespread formation of new ice within the Beaufort. Thin ice types reached a peak regional concentration of 30% in March, when the ice cover is typically dominated by thick first-year and multiyear sea ice. Combined CryoSat-2 and Soil Moisture and Ocean Salinity (SMOS) data indicate that the regional ice volume plateaued from December to March as export offset ice growth and ultimately culminated in a −30% volume anomaly in April 2016. This atypically thin ice cover broke up 7 weeks earlier than average, with open water forming not only within coastal flaw leads but also within the offshore pack ice. By July 2016, vast areas of open water within the highly fractured ice cover accelerated the ice-albedo feedback and led to rapid melt. Though maintaining a partial ice cover during summer throughout the observational record, significant negative trends in September sea ice area within the Beaufort are now punctuated by two recent ice-free Septembers (2012 and 2016). As the Beaufort transitions toward a seasonally ice-free sea, we examine the role of winter preconditioning through sea ice transport and its growing importance within an increasingly seasonal and mobile Arctic ice cover.

**Plain Language Summary** During September 2016 the Beaufort Sea became ice-free for the second time in 5 years after it had historically maintained a partial ice cover throughout the observational record. September sea ice area in the Beaufort has significantly declined, and while the region continues to completely freeze over during winter, the composition of this ice cover is changing. The Beaufort is transitioning from an ice cover dominated by multiyear sea ice to one characterized by thinner first year ice types. This thinner ice cover is less resilient to summer melt and is also mechanically weaker and therefore more mobile. As a result, the ice cover is more prone to large fracture events that lead to new ice formation during winter and precondition the end of winter ice cover for enhanced summer melt. Within this paper, we focus on a series of events during winter 2016 that broke up the ice cover and preconditioned it toward younger and thinner ice types. Ultimately, this promoted early breakup, which enhanced summer melt and ultimately rendered the region ice-free by September 2016. Building on this, we find a statistical relationship between winter ice export and summer ice loss.

## 1. Introduction

Winter 2015–2016 in the Arctic was characterized by warm air temperatures (Cullather et al., 2016), reduced thermodynamic ice growth (Ricker, Hendricks, Girard-Ardhuin et al., 2017), and record low monthly sea ice extents (Petty et al., 2018). While the September 2016 hemispheric sea ice minimum ($4.72 \times 10^6$ km$^2$) did not reach a record low, regionally, the Beaufort Sea became completely ice-free (Figure 1a). This was the second time in 5 years that the Beaufort Sea had become ice-free after it had historically maintained a partial ice cover during summer throughout the observational record. From 1979 to 2018 there has been a significant ($p < 0.05$) negative trend of −5,236 km$^2$/year in September sea ice area within the Beaufort Sea (Figure 1b). However, a clear transition in the ice area record occurred in 1998 (Hutchings & Rigor, 2012). Prior to 1998 September sea ice area varied around the 19-year mean of 215,780 ± 69,480 km$^2$ with no

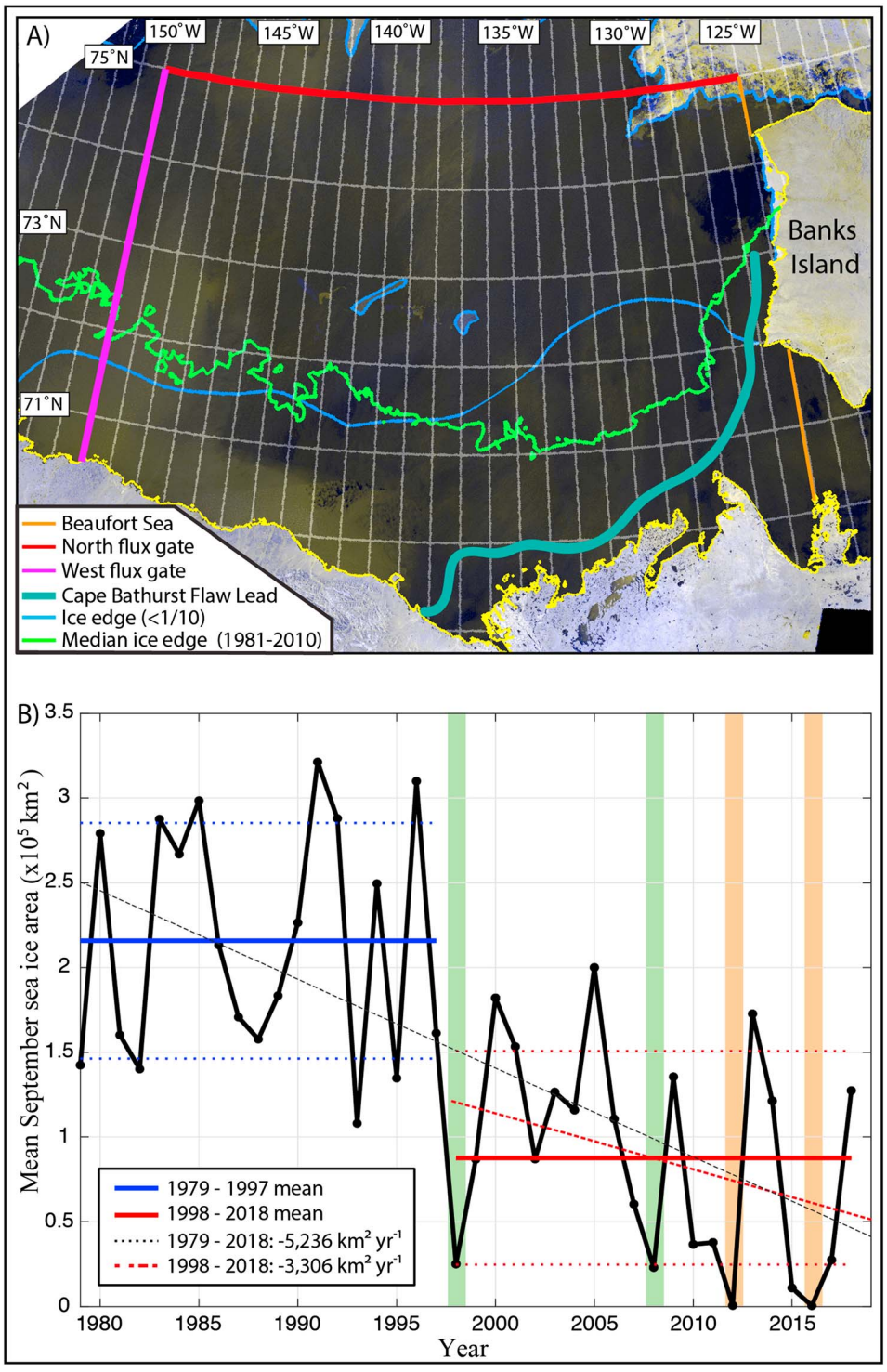


**Figure 1.** (a) Radarsat mosaic over the Beaufort Sea from 16 to 19 September 2016. Mosaic compiled by the Canadian Ice Service (hhtp://www.ec.gc.ca/glaces-ice; Luo & De Abreu, 2010). The Beaufort Sea is bounded by 150°W to the west, 75°N to the north, 125°W and Banks Island to the east, and continental North America to the south. The green line denotes the historic median ice edge (1981–2010). The thick teal line denotes the approximate location of the Cape Bathurst Flaw Lead Polynya (Barber & Hanesiak, 2004). (b) Mean September sea ice area ($km^2$) in the Beaufort Sea from the NASA Team Algorithm (Cavalieri et al., 1996). The 1979 to 1997 mean ± 1 standard deviation is represented by blue lines. The 1998–2018 mean ±1 standard deviations is represented by red lines. The 1979–2018 trend is presented by the black dashed line, while the 1998–2018 trend is presented by the red dashed line. The green and orange shading highlight the four Beaufort minima.

underlying trend (Figure 1b). Whereas from 1998 to 2018, the mean September ice area fell to 87,709 ± 63,083 $km^2$ with an underlying negative trend of −3,308 $km^2$/year (Figure 1). The reduction in September sea ice area was punctuated in 2012 when the Beaufort Sea first became ice-free (Babb et al., 2016). The regional ice cover recovered somewhat during 2013 as a result of high sea level pressure that led to convergent ice drift against the Canadian Arctic Archipelago (Howell et al., 2016; Kwok, 2015) and cool air temperatures that limited surface melt and maintained a high surface albedo throughout summer 2013 (Kwok, 2018). This created a thick ice cover during winter 2014 (Tilling et al., 2015) and allowed the recovery of the ice cover to persist through summer 2014 (Figure 1b). However, the recovery was short-lived and the Beaufort Sea once again became ice-free during September 2016.

The ice cover of the Beaufort Sea is comprised of a mix of new ice, first year sea ice (FYI), and multiyear sea ice (MYI; Galley et al., 2016, 2008). New ice represents the initial formation of sea ice in areas of open water and quickly develops into FYI, which continues to grow thicker throughout winter. During freeze-up, new ice forms wherever there is not an existing ice cover. However, following the formation of a complete regional ice cover, new ice formation is confined to areas of open water that form within leads in the pack ice, and larger areas of open water exposed by the dynamic opening of the Cape Bathurst flaw lead system along the landfast ice edge in the southeastern Beaufort Sea (Figure 1a; Barber & Hanesiak, 2004; Galley et al., 2016, 2012, 2008). Conversely, MYI is either advected into the Beaufort Sea by the anticyclonic Beaufort Gyre (Howell et al., 2016) or developed within the Beaufort from FYI that persists through summer into the following winter. Since the 1980s there has been a northward retreat of the MYI edge within the Beaufort Sea (Galley et al., 2016) as a greater percentage of MYI now melts out within the Beaufort during summer (Kwok & Cunningham, 2010; Maslanik et al., 2011; Stroeve et al., 2011). This change exposes an increasingly large area of open water for the formation of new ice during fall and growth of FYI throughout winter. Overall the Beaufort Sea is becoming covered by a more seasonal ice cover (Galley et al., 2016) that is weaker and more responsive to atmospheric forcing, making the ice cover more mobile and dynamic (e.g., Kwok et al., 2013; Rampal et al., 2009). In particular, Petty et al. (2016) found that sea ice within the Beaufort Sea has become increasingly responsive to surface winds, especially during the late 2000s, which has driven increased westward ice transport from the Beaufort Sea into the Chukchi Sea. Westward ice transport is typically greater than northern import (Howell et al., 2016; Petty et al., 2016) creating an imbalance that leads to the formation of open water and new ice growth during winter, drives the start of breakup in the eastern Beaufort Sea during spring (Galley et al., 2008; Steele et al., 2015), and contributes to the regional loss of sea ice during summer that in turn amplifies the ice albedo feedback. Beyond increased ice export, the transition to a more mobile ice cover has also made the Beaufort Gyre more prone to reversals (Lukovich & Barber, 2006) during which sea ice may be imported from the Chukchi Sea and cause the Beaufort ice cover to converge as it is constrained to the east by Banks Island. This convergence can lead to deformation of the ice cover and prevent new ice formation during winter, though the affect may be greatest during summer when reversals can consolidate the ice cover and limit ice melt. A prolonged reversal of the Beaufort Gyre occurred during winter 2017 (Moore et al., 2018a), and while the reversal was driven by the collapse of the Beaufort High as a result of cyclonic intrusions from the Atlantic sector of the Arctic Ocean, the reversal was undoubtedly amplified by the presence of a more mobile seasonal ice cover following ice free conditions during September 2016 (Figure 1).

Underlying the significant negative trend in observed September sea ice area within the Beaufort Sea is several clear sea ice minima (1998—Maslanik et al., 1999, 2008—Perovich et al., 2011, and 2012—Babb et al., 2016), which have all been related to an accelerated ice albedo feedback that was initialized by premature breakup of the regional ice cover. By breaking up earlier than average the ice cover exposed a greater area of open water around the seasonal peak in downwelling solar radiation that promoted heating of the upper ocean and amplified ice melt. While the Beaufort ice cover has been trending toward an earlier breakup date (Frey et al., 2015; Galley et al., 2016), the Beaufort ice cover broke up noticeably earlier during years that subsequently had low September sea ice concentrations (Babb et al., 2016). Earlier than average breakup during 1998, 2008, and 2012 has been directly attributed to the presence of younger and thinner ice types during the preceding winter (Babb et al., 2016; Perovich et al., 2011).

Prior to the 1998 regional sea ice minimum, the Beaufort Gyre circulated younger sea ice into the Beaufort Sea during 1997 (Rigor & Wallace, 2004), which promoted ice melt, specifically MYI melt, in the western Arctic during summer 1997 (Kwok & Cunningham, 2010) and reduced the presence of MYI in the

Beaufort Sea during fall 1997 (McPhee et al., 1998). This preconditioned the ice cover of winter 1998 toward younger and thinner ice types, which was then amplified by persistent southerly and easterly winds during winter that advected the remaining MYI out of the Beaufort Sea (Maslanik et al., 1999). Ultimately, by the start of the 1998 melt season the Beaufort ice cover was predominantly comprised of seasonal ice types (Canadian Ice Service ice charts—not shown) that created negative ice thickness anomalies in the southern Beaufort Sea (Melling et al., 2005) and ultimately encouraged early breakup and rapid melt through summer 1998 (Babb et al., 2016).

Similarly, the 2008 sea ice minimum can be related back to preconditioning from the previous summer. During the record September 2007 sea ice minimum, the regional sea ice area fell to its second lowest value (Figure 1b). Negative sea ice anomalies throughout spring and summer 2007 increased solar absorption throughout the Beaufort Sea and drove an accelerated ice albedo feedback that increased bottom melt (Perovich et al., 2008; Steele et al., 2010). By the end of summer 2007 there was only a concentrated MYI ice cover remaining in the central Beaufort Sea (Canadian Ice Service ice charts—not shown). While these processes were not strong enough to completely melt the entire ice cover, they did delay fall freeze-up (Comiso et al., 2008) and led to the formation of a near-surface temperature maximum (Jackson et al., 2010) that reduced ice growth by 25% during the subsequent winter (Timmermans, 2015) leaving the ice cover at the end of winter 2008 thinner than average. This contributed to the early breakup and accelerated ice albedo feedback that increased bottom melt (Perovich et al., 2011) and total melt (Kwok & Cunningham, 2010) during summer 2008 and ultimately led to the then-lowest recorded mean September sea ice area within the Beaufort Sea (Figure 1b).

The regional September sea ice minimum of 2008 was surpassed in 2012 when the entire Beaufort Sea was ice-free for 31 consecutive days (Babb et al., 2016). On a hemispheric scale the 2012 sea ice minimum was attributed to decadal scale preconditioning of the ice pack toward thinner and younger ice types (Parkinson & Comiso, 2013; Zhang et al., 2013), warm surface waters (Zhang et al., 2013), and the added influence of a late summer cyclone (Simmonds & Rudeva, 2012) that dispersed the ice pack and enhanced bottom melt (Zhang et al., 2013). Regionally, increased seasonal ice coverage within the Beaufort Sea during the preceding winter (Parkinson & Comiso, 2013) created a more mobile ice cover that enabled greater divergence and export out of the Beaufort Sea during spring (Nghiem et al., 2014). This, in turn, exposed areas of open water and initiated the ice albedo feedback (Babb et al., 2016).

While there are many factors that dictate how sea ice is lost during summer, in the Beaufort Sea there appears to be a relationship between enhanced winter dynamic activity and accelerated summer thermodynamic melt that punctuates the overall declining trend of summer sea ice area with years of extreme ice loss. Historically, the MYI-dominated ice cover of the Beaufort Sea was not appreciably affected by atmospheric forcing as the thick and mechanically strong ice cover remained quiescent during winter. However, following 1998, the Beaufort ice cover was increasingly comprised of seasonal ice (Hutchings & Rigor, 2012) and following the 2007 sea ice minimum, the Beaufort has transitioned toward a predominantly seasonal ice cover (Galley et al., 2016). This transition has made it more responsive to atmospheric forcing (Petty et al., 2016), which has contributed to three notable sea ice minima within a decade containing three of the eight lowest recorded regional September sea ice areas (Figure 1b). Previous work has shown that winter dynamics do condition the ice cover for enhanced summer ice loss, but within this work we build on those previous studies by using an extensive suite of remotely sensed observations of sea ice type, concentration, thickness, and drift to examine this process. Specifically, we focus on the winter of 2016, examining how sea ice transport influenced the regional ice cover in terms of ice type and volume and how this conditions the ice cover for summer melt. Subsequently, we set the 38-year context of ice transport and 5-year context of ice volume to highlight how larger scale changes to the Arctic and the Beaufort in particular are promoting this dynamic preconditioning process and in turn promoting summer ice loss. Finally, we explore the potential for a predictive relationship between winter ice dynamics and September sea ice area at the regional scale.

## 2. Methods

We have employed a combination of remotely sensed fields of ice type, concentration, drift, and thickness, coupled with atmospheric reanalysis products. Each dataset is described below.

### 2.1. Canadian Ice Service Ice Charts

The Canadian Ice Service (CIS) produces weekly ice charts (freely available at http://iceweb1.cis.ec.gc.ca) that represent sea ice concentration by stage of development using the World Meteorological Organization egg code. The ice charts delineate different ice regimes with polygons that present the partial concentration (tenths) of up to three different stages of development. Polygons are defined by expert manual interpretation of remotely sensed imagery and ship and air borne observations (Fequet, 2005). Since 1996, RADARSAT-1 and subsequently RADARSAT-2 have been the primary data source for the CIS (Tivy et al., 2011). Within this analysis, we distinguish between MYI, thick FYI (>120 cm), medium FYI (70–120 cm), and thin FYI (30–70 cm), while we group new (<10 cm) and young (10–30 cm) ice types into a single class referred to as "new ice." Furthermore, we refer to thin FYI and new ice as "thin ice" types. In order to ensure areas of new ice were classified consistently across ice charts we only consider ice charts produced since 1996 when Radarsat-1 and -2 have been the primary data source for CIS ice analysts. Differentiation between thin, medium, and thick FYI types is based on the expert manual interpretation of the available observations and context provided by regional air temperatures that drive a simple freezing degree-day model (Agnew & Howell, 2003). Note that the ice thickness range associated with each ice type is an approximation and not an actual measure of ice thickness. The CIS ice charts have always been an operational product first and foremost, and as such, from November to May, they were historically only produced for the first of every month. However, from November 2005 to May 2006 ice charts were produced biweekly, and since 2007 they have been produced weekly for each month of the year. As a result, our 2016 analysis presents weekly ice type data, but our historical context is limited to the start of each month. Further details on the processing of the ice charts and their applicability are discussed in Galley et al. (2016) and Tivy et al. (2011). Weekly RADARSAT image mosaics (e.g., Figure 1a) produced by the CIS (Luo & De Abreu, 2010) are also presented within this study.

### 2.2. Sea Ice Concentration, Drift, and Flux

Daily fields of sea ice concentration and ice drift were retrieved from the National Snow and Ice Data Center (NSIDC). Sea Ice Concentrations from Nimbus-7 SMMR and DMSP SSIM/I-SSMIS Passive Microwave Data (Version 1; Cavalieri et al., 1996; updated 2016), which uses the National Aeronautics and Space Administration (NASA) team algorithm, were used to derive sea ice area within the Beaufort Sea. Note that from 1979 until 20 August 1987, sea ice concentration fields were only available every second day, so a sliding 3-day mean was used to fill in missing data. In terms of ice drift, the Polar Pathfinder Daily 25 km EASE-Grid Sea Ice Motion Vectors (Version 3; Tschudi et al., 2016) were used to analyze ice drift and divergence within the Beaufort Sea and quantify ice transport across the northern (150°W; purple line Figure 1a) and western (75°N; red line Figure 1a) gates of the Beaufort Sea, as defined by Babb et al. (2016), from 1979 to 2016. Vector data are provided as components ($u$ – zonal, $v$ – meridional) and are used to calculate the daily and monthly divergence ($D$) of the Beaufort ice pack from the following equation presented by Kwok (2001) and used within Landy et al. (2017),

$$D = \left(u_x + v_y\right)/2 \tag{1}$$

The daily ice flux ($F_i$; km$^2$/day) was calculated at 5-km intervals along the western and northern gates of the Beaufort Sea from the following equation,

$$F_i = \Sigma\, c_i\, u_i\, \Delta x \tag{2}$$

where $c_i$ is the daily sea ice concentration interpolated to each point, $u_i$ is the daily ice velocity component normal to the gate (zonal velocity for the west gate, meridional velocity for the north gate) interpolated to each point, and $\Delta x$ is the interval of points along the gate (5 km). The sum of $F_i$ along each gate is referred to as the western and northern flux, while the sum of these two fluxes is presented as the net ice transport. Positive fluxes represent ice import to the Beaufort Sea, whereas negative fluxes represent ice export from the Beaufort Sea. The cumulative net ice transport from January through April is calculated for each year. Similarly, cumulative ice transport during the melt season is calculated from the day that the regional sea ice concentration fell and remained below 95% (start of breakup) to the September minimum and used to infer the contribution of ice melt and ice transport to regional summer ice loss. Kwok (2008) applied this method to summer ice loss in the Pacific sector of the Arctic but used monthly ice fluxes from June to

September. Provided that ice transport drives the initial reduction in regional sea ice area within the Beaufort Sea (Steele et al., 2015), we dynamically define breakup and consider ice transport during the entire period of ice loss. Within this calculation, it is important to note that ice export from Amundsen Gulf into the southern Beaufort Sea is not considered, as the data used within this analysis do not resolve ice drift between Cape Tatnam and Banks Island. Therefore, our estimates of regional ice melt are conservative as additional sea ice is typically flushed out of Amundsen Gulf into the Beaufort Sea during the start of the melt season before the Amundsen Gulf ice flux declines to zero during July, August and September (Kwok, 2006b).

Vectors near coastlines (typically within 25 km) are noted for potential coastal contamination and are not considered within our ice flux calculations. Due to the location of our ice flux gates, coastal contamination is limited to the southern end of the western gate and led to the exclusion of the first ten points along the flux gate. Excluding these 10 points reduced the average daily ice flux across the western gate by 105 $km^2$ between January and April from 1979 to 2016. In terms of the cumulative January to April ice flux the difference was on average −7,270 $km^2$ or 5% of the cumulative western ice flux. As a result ice flux calculations across the western gate should be considered a conservative estimate. Following Kwok and Rothrock (1999) and subsequently Howell et al. (2016), the uncertainty in $F_i$ ($\sigma_f$) is calculated from the following equation:

$$\sigma_f = \left(\sigma_e/\sqrt{N_s}\right) L \tag{3}$$

where $\sigma_e$ is the error in the Polar Pathfinder dataset, *Ns* is the number of sampling points along each gate (88 western and 142 northern), and *L* is the length of the gate (440 km western and 710 km northern). Sumata et al. (2014) found that of four different remotely sensed ice drift products available the Polar Pathfinder dataset had the highest correlation with ice beacon data and the lowest error. This is to be expected because the ice beacon data are integrated into the maximum cross correlation method applied to derive the ice drift vectors (Tschudi et al., 2016). Regardless, the error in ice drift was found to be lower during winter (December to April; $\sigma_e$ = 1.01 cm/s or 0.873 km/day) compared to summer (May to October; $\sigma_e$ = 1.30 cm/s or 1.123 km/day; Sumata et al., 2014). Therefore, the estimated uncertainty of ice flux across the northern gate is 52 $km^2$/day during winter and 67 $km^2$/day during summer, and for the western gate the uncertainty is 41 $km^2$/day during winter and 56 $km^2$/day during summer. In terms of the net January to April ice flux these correspond to uncertainties of 6,240 $km^2$ across the northern gate and 4,920 $km^2$ across the western gate.

### 2.3. Atmospheric Reanalysis

Daily fields of sea level pressure (SLP), surface air temperature, and surface winds from the National Oceanic and Atmospheric Administration's (NOAA) National Center for Environmental Prediction's (NCEP) reanalysis 2 dataset (Kanamitsu et al., 2002) were used to examine the atmospheric forcing over the Beaufort Sea. Daily mean SLP (mb) and zonal winds (m/s) were calculated over the Beaufort Sea (70–75°N; 125–150°W), while a northeast (75°N, 135°W) to southwest (67.5°N, 155°W) SLP index that bisects the mean field of motion (Rigor & Wallace, 2002) was calculated across the Beaufort Sea as an indication of the strength and orientation of the isobars that drive surface winds and therefore ice drift.

### 2.4. Sea Ice Thickness and Volume

Weekly fields of sea ice thickness derived from the radar altimeter Cryosat-2 and the L-band radiometer SMOS (Soil Moisture and Ocean Salinity-CS2/SMOS; Ricker, Hendricks, Kaleschke et al., 2017) are used to explore the spatial pattern of ice thickness and time series of ice volume in the Beaufort Sea. Ice thickness data from these two satellites differ in spatial and temporal resolution, with SMOS providing complete daily coverage of the Arctic at coarse resolution and only over areas of thin ice (<50 cm), whereas CS2 provides higher along track resolution but with limited spatial coverage and is more accurate over thicker ice types with greater freeboard. Hence, an optimal interpolation method is used by Ricker, Hendricks, Klaeschke et al. (2017) to merge these two datasets and produce weekly fields of ice thickness over the northern hemisphere at 25-km resolution. The merged dataset was validated against in situ airborne observations of ice thickness, which revealed that merging CS-2 with SMOS provides greater accuracy over areas of thin ice compared to just the CS2 dataset (Ricker, Hendricks, Klaeschke et al., 2017). The dataset spans late October to mid-April of each year since October 2010 and uses the modified Warren snow climatology (Warren et al., 1999) to calculate ice thickness based on the OSI SAF ice type product (Eastwood, 2012).

Sea ice volume is calculated based on the sea ice concentration provided within the dataset that was in turn calculated from the OSI SAF sea ice concentration product (Eastwood, 2012). While the coarse spatial resolution of SMOS precludes it from detecting thin ice in narrow leads, the vast areas of thin ice identified within the CIS ice charts over the Beaufort Sea during winter 2016 are clearly evident within the daily SMOS fields and display how suitable the dataset is for this analysis.

### 2.5. Solar Absorption Through Areas of Open Water

Daily fields of sea ice concentration and downwelling solar radiation at the surface were used to estimate the daily solar absorption through areas of open water ($F_{ow}$) within the Beaufort Sea according to the following equation:

$$F_{ow} = F\,(1-\alpha)\,A_{ow} \tag{4}$$

where $F$ is the surface solar irradiance (W/m$^2$), α is the albedo of open water (0.07), and $A_{ow}$ is the fractional area of open water (1-$c_i$). $A_{ow}$ was derived from the NSIDC fields of sea ice concentration data described above. Fields of surface solar radiation downward were retrieved from the ERA-Interim reanalysis of the European Center for Medium-range Weather Forecasts (ECMWF; Dee et al., 2011). Of the various reanalysis products available, ERA-Interim was chosen because it has shown an improvement in the seasonal and interannual variability of solar radiation over its predecessor ERA-40 (Balmaseda & Mogensen, 2010), which was already found to be the most accurate reanalysis product in terms of solar radiation (Walsh et al., 2009). Solar absorption through areas of open water has a direct relationship to ice melt along the bottom of the ice cover (Perovich et al., 2011) and has driven increased bottom melt within the Beaufort Sea as a result of an amplified ice albedo feedback (Babb et al., 2016; Perovich et al., 2008). Therefore, solar absorption during the melt season is used to infer bottom melt and explain the regional loss of sea ice.

## 3. Results

### 3.1. 2015-2016 Sea Ice Season

The 2015–2016 sea ice season in the Beaufort Sea began with the onset of new ice formation in late-September 2015 following a regional minimum sea ice concentration of 16% (Figure 2; note that the sea ice concentration from the ice charts is greater than from the passive microwave record presented in Figure 1b (Agnew & Howell, 2003)). Prior to the onset of new ice formation, the Beaufort ice cover was solely comprised of MYI, which continued to decline to a minimum regional concentration of 10% at the end of September (Figure 2a). New sea ice formation progressed rapidly during October until the Beaufort Sea was nearly 100% ice covered by the first week of November 2015 (Figure 2a). While the Beaufort Sea remained completely ice covered until late April, the composition of the ice pack evolved and changed considerably throughout winter (Figure 2a). MYI concentrations increased steadily from 10% at the end of September to 38% in May (Figure 2a). Seasonal ice types progressed from new to thin, medium, and thick FYI, while the Cape Bathurst flaw lead maintained a small portion of new ice throughout December and January (Figure 2). At the start of January the Beaufort ice cover was typical of the last decade, with MYI and medium FYI comprising 80% of the ice pack and a combination of new and thin FYI making up the remaining 20% (Figure 2b). By the end of January thin ice types were confined to pockets of the coastal flaw lead system (Figure 3; 25 January) as the regional concentration of thin ice types reached its seasonal minimum (Figure 2a). New ice formation during early February increased the regional concentration to 7%, which was a 20-year peak for the month of February (Figure 2c), while continued new ice formation increased the regional concentration to 15% by mid-February (Figure 2a). The rapid increase in new ice concentrations was due in part to the opening of the coastal flaw lead system but also reflects the formation of large areas of new ice, in concentrations of up to 9+ tenths within the mobile ice cover (Figure 3; 15 February). These regions were generally elongated, extending across the Beaufort Sea from north to south, and parallel to the western coast of Banks Island. By the first week of March, 27% of the Beaufort ice cover was comprised of thin ice types. This is 9 times greater than the 20-year mean of 3%, 3 times greater than the previous peak of 9% during 2008 and 2013, and far different than the MYI and thick FYI dominated ice pack that has climatologically covered the Beaufort during March (Figure 2d). On 7 March, the concentration of thin ice types reached a seasonal peak of 30%, and while new ice was limited to the flaw lead system, thin FYI pervaded the Beaufort Sea in concentrations of up to 9+ tenths (Figure 3; 7 March). By the first week of April

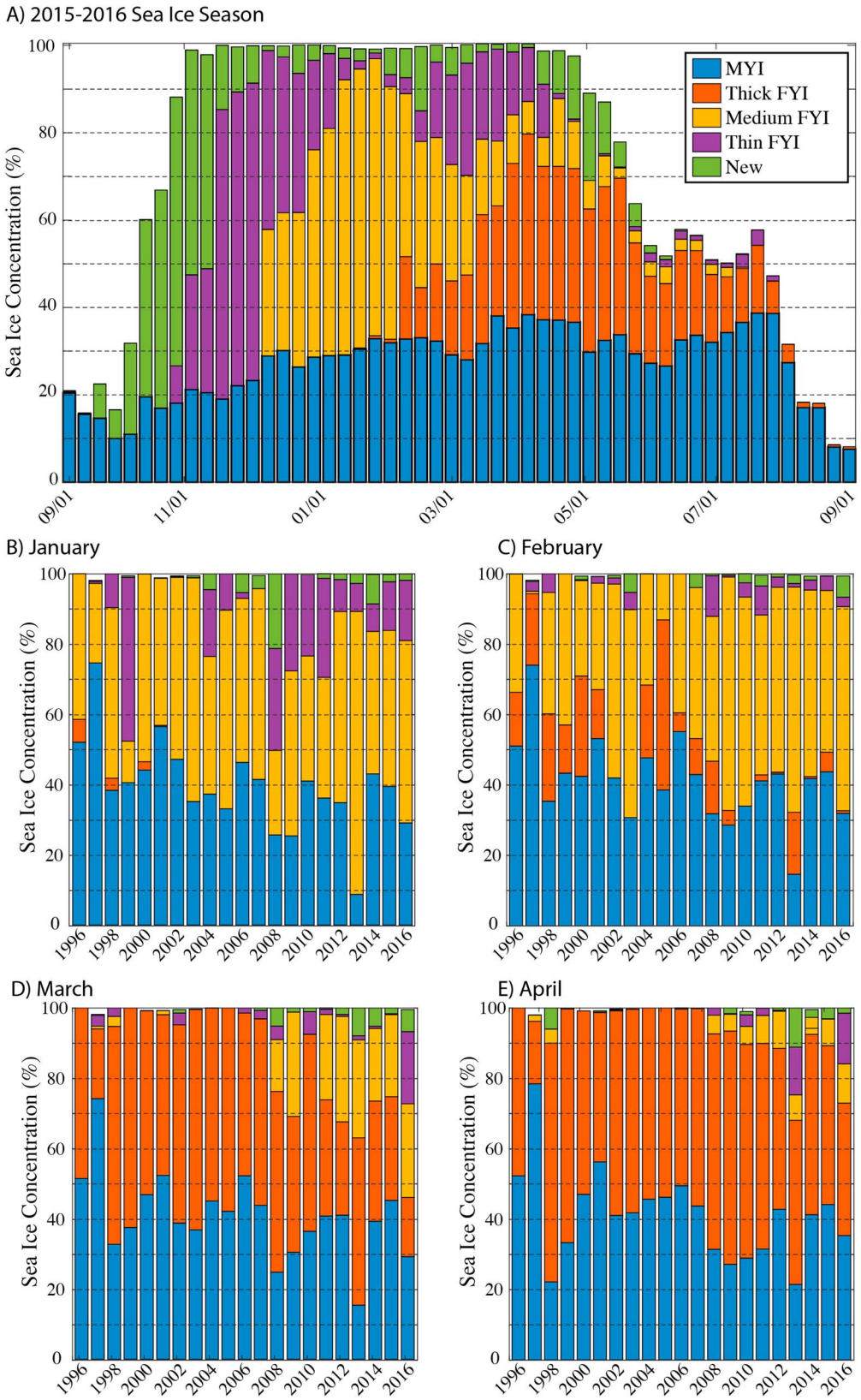


**Figure 2.** Regional sea ice concentration by ice type in the Beaufort Sea from the Canadian Ice Service ice charts. (A) During the 2015–2016 sea ice season. (b–e) During the first week of January, February, March, and April from 1996 to 2016.

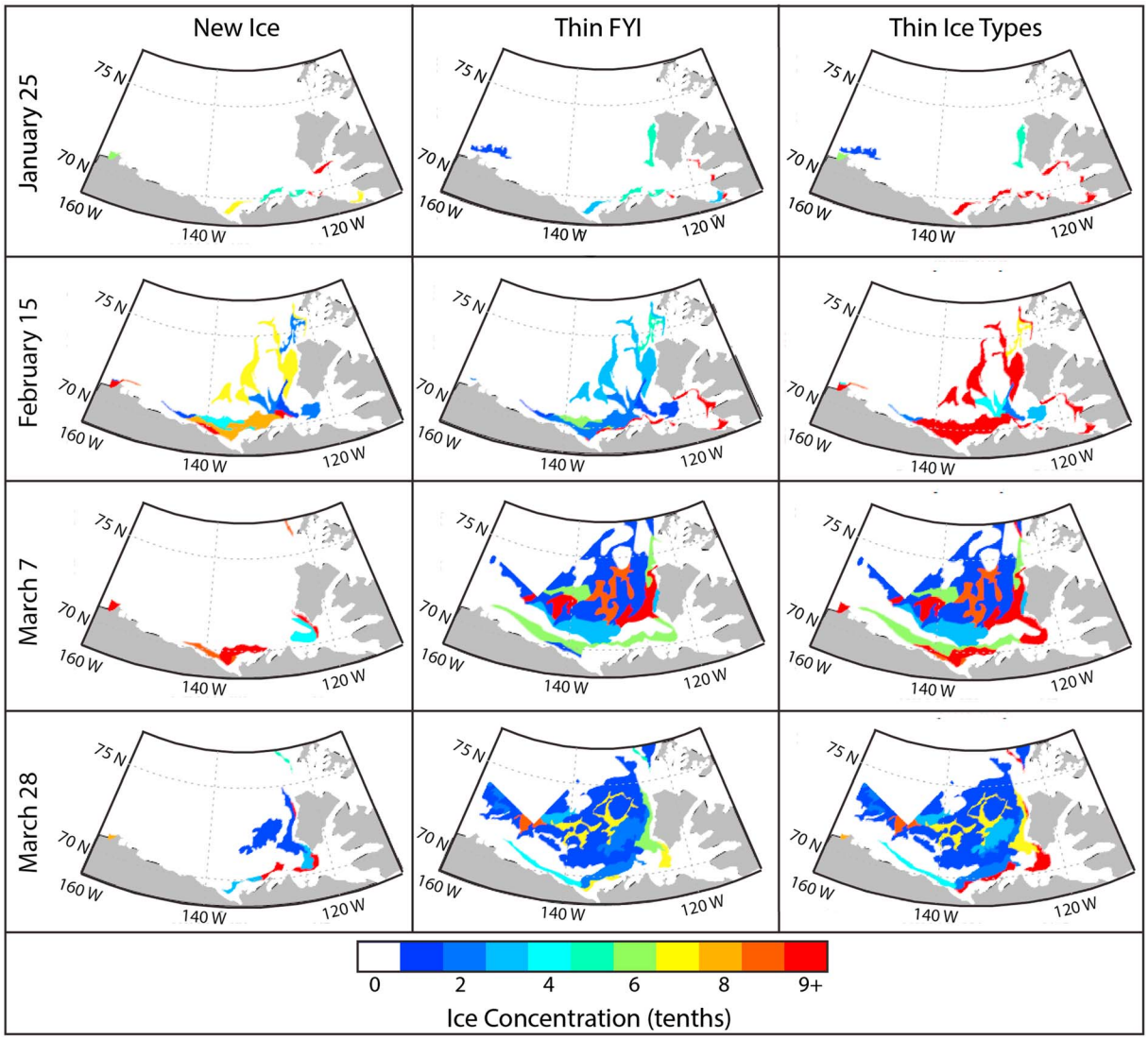


**Figure 3.** Maps of the partial concentration (tenths) of new ice (left column), thin FYI (middle column) and the combination of the two thin ice types (right column) from 4 Canadian Ice Service ice charts during winter 2016.

seasonal ice types had thickened and the regional concentration of thin ice types had declined from a mid-March peak of 30 to 17% (Figure 2a). Historically, from 1996 to 2015 the average composition of the Beaufort ice cover during the first week of April was 41% MYI, 53% thick FYI, 3% medium FYI, and 3% thin ice types. The presence of thin ice types during 2016 was 5 times greater than the climatological mean, and greater than every year except for 2013, which appeared to be preconditioned for rapid summer melt; however, this did not occur, for reasons discussed below. Overall, by the end of winter 2016 thin ice types were much more prevalent within the Beaufort ice cover and had thereby conditioned the ice cover for increased summer melt.

Following the first week of April 2016, the unusually young ice cover in the Beaufort Sea began to breakup, disrupting the complete ice cover and leading to the persistent presence of open water (Figure 2). Typically, open water first appears in the coastal flaw lead zones and expands offshore into the mobile ice pack as spring progresses. However, by early May 2016 the Beaufort ice cover was heavily broken up, and vast areas of open water had formed (Figure 4a) where thin ice had previously been located (Figure 3). Subsequently, the regional sea ice concentration declined rapidly during May, as seasonal ice types melted preferentially (Figure 2a). While MYI concentrations declined slightly during May, they were replenished during June

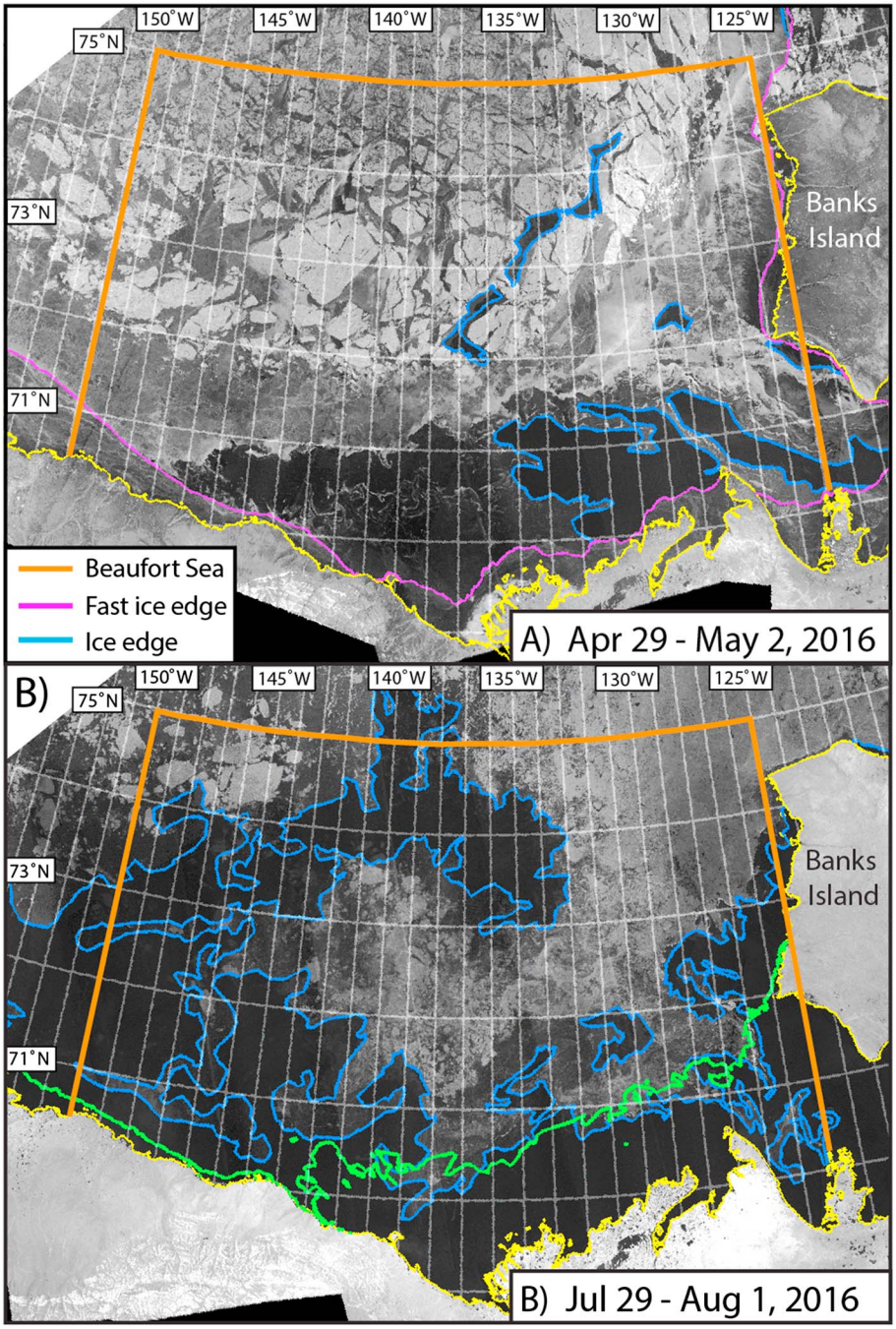


**Figure 4.** Radarsat Mosaics over the Beaufort Sea from (a) 29 April to 2 May 2016 and (b) 29 July to 1 August 2016. The blue line denotes the ice edge and areas of open water.

and July, which contributed to a stabilization of the regional sea ice concentration around 50% (Figure 2a). However, by August 2016, the ice cover was interspersed in low concentrations with areas of open water (Figure 4b) and declined rapidly until only a small patch of concentrated sea ice remained in the northeast Beaufort Sea along the west coast of Banks Island (Figure 1a).

### 3.2. Winter Dynamics in the Beaufort Sea

The formation of new ice within a highly concentrated winter ice pack requires open water either be created by the regional export of sea ice or local sea ice divergence. Either way the ice cover must become mobile at a

time of year when it is typically least mobile. Hence, we examine the atmospheric forcing and resultant ice drift from January through to April 2016, when new ice formed within the Beaufort ice cover (Figure 5). Both the weekly CIS ice charts and daily SMOS-derived fields of ice thickness show the midwinter and early spring increase in the presence of thin ice within the Beaufort Sea (Figure 5a). The concentration of new ice (Figure 5a, green shaded) increased considerably during five separate weeks. The first 3 weeks of new ice formation occurred during late-January and February (yellow shading) within the highly concentrated winter ice cover and under a cold overlying atmosphere (Figures 5a and 5b). The latter two occurred in April (pink shading) and in conjunction with warming air temperatures fostered the formation of areas of open water (black) within the Beaufort Sea (Figures 5a and 5b).

The first three new ice formation events have very little relation to the time series of mean SLP (Figure 5c) over the Beaufort Sea; the SLP was low during the first event, high during the second event, and moderate during the third event. Given that ice drift is not simply driven by the magnitude of SLP over a region but instead the relative gradients and orientation of isobars, the daily SLP index across the Beaufort Sea identifies periods of strong atmospheric forcing relevant to export and/or divergence. From January to April the SLP Index exceeded 25 mb five separate times, each of which corresponds to the seasonal peaks in easterly winds (green line, Figure 5d) and westward ice drift (black line, Figure 5d), which drove increased ice export out of the Beaufort Sea through its western gate (red line, Figure 5e). Western ice export was only partially offset by sea ice import across the northern gate (blue line, Figure 5e), leading to a negative cumulative ice balance within the Beaufort Sea (green line, Figure 5e) that encouraged the formation of areas of open water where new ice subsequently formed (Figure 5a). From January to April 2016 there was a net ice export of 343,630 $km^2$ through the Beaufort Sea, which is the greatest cumulative ice export over this 4-month period for the 38-year period of observations and over 5 times greater than climatological mean export of 68,250 $km^2$ (Figure 5e). Furthermore, instead of the ice cover being transported westward coherently as a consolidated ice pack and limiting areas of open water to the flaw lead along Banks Island, it fractured and diverged (Figure 5f) creating areas of open water where new ice formed within the Beaufort ice pack. Over winter, cold atmospheric temperatures led to the rapid formation of new ice, whereas during late-April rising air temperatures (Figure 5b) precluded new ice formation and allowed open water to persist in divergent regions (Figure 5a).

Based on the 5 weeks of pronounced new ice formation we have identified in Figure 5a, we separate the January to April 2016 time frame into four periods for further analysis (Figure 6). The first (1 to 25 January) and third (1 March to 4 April) periods are characterized by a weak SLP gradient across the Beaufort Sea that led to reduced ice drift speeds, relatively low western ice export (Period 1: 2,949 $km^2$/day; Period 3: 2,712 $km^2$/day), limited divergence within the Eastern Beaufort Sea (Figure 6) and reduced presence of thin ice types (Figure 5a). During both periods, there were reversals to westerly winds and eastward ice drift, which corresponded to ice import across the western gate and convergence within the ice cover (Figure 6). Furthermore, underlying the gradual reduction in thin ice extent during Period 3 were two pronounced reversal events in mid-March and early-April (Figure 5d) that both caused the extent of thin ice to decline (Figure 5a). During periods of convergence, we expect newly formed thin ice—deformed far more easily than thick sea ice floes—to decrease in extent, as the ice is dynamically broken, compressed, and thickened.

Conversely, the second (26 January to 29 February) and fourth (5 to 30 April) periods were characterized by strong SLP gradients across the Beaufort Sea that enhanced ice drift speeds, increased western ice export (Period 2: 5,908 $km^2$/day; Period 4: 5,776 $km^2$/day), led to considerable divergence within the Eastern Beaufort Sea (Figure 6), and increased the presence of thin ice (Figure 5a). It is important to note that phases of high export across the western gate during Periods 2 and 4 do not experience equally high ice import across the northern gate. Rather, while western export is high, the net flux across the northern gate is close to zero, leading to strong divergence within the region, with phases of high ice import across the northern gate lagging behind by ~1 week. Hence, ice import from the Central Arctic did not dynamically fill in open water areas in the Beaufort Sea, which allowed significant fractions of new ice to form. There were no reversals in ice drift during Periods 2 and 4 and, as a result, there was near-continuous ice export and divergence (Figure 5), which collectively opened up the ice pack and enabled the formation of new ice in the eastern Beaufort Sea. The ice drift data clearly indicate that divergence is confined to the eastern and northern Beaufort Sea, while the ice cover converges around and upstream of the shear zone near Point Barrow

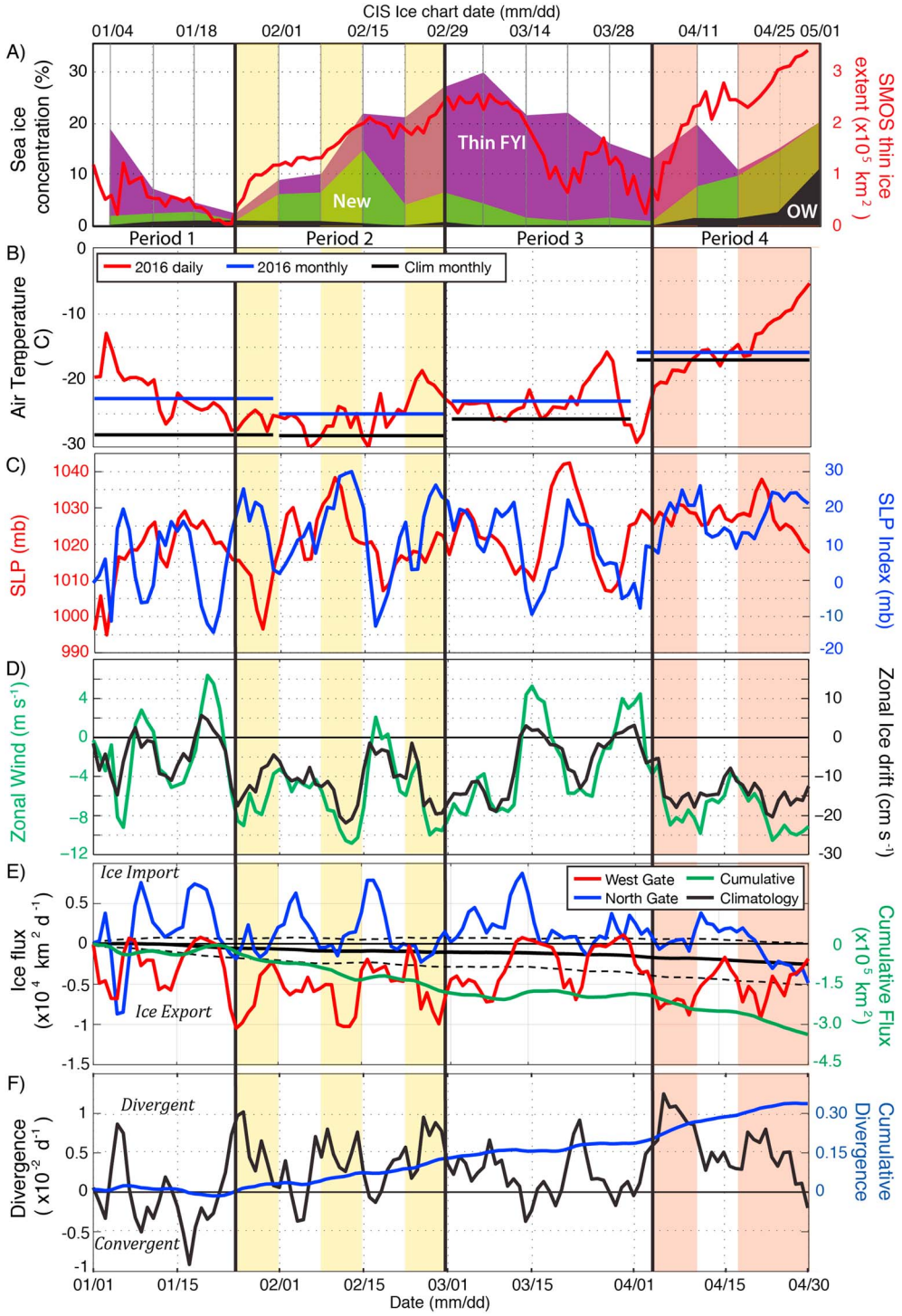


**Figure 5.** Time series from 1 January to 1 May 2016 of the (aa) partial concentration of thin ice types from the Canadian Ice Service (CIS) ice charts and Soil Moisture and Ocean Salinity (SMOS) daily fields of thin ice thickness (<0.5 m; green); (b) National Center for Environmental Prediction (NCEP) daily air temperature (red), monthly mean (blue), and climatological monthly mean (black); (C) sea level pressure (SLP; red) and the SLP index (blue) across the Beaufort Sea; (d) zonal wind (green) and ice drift speed (black) within the Beaufort Sea; (e) ice flux across the western (red) and northern (blue) gates, the daily net flux (black), and the cumulative net flux (green) through the Beaufort Sea; (f) daily (black) and cumulative (blue) divergence of the ice pack within the Beaufort Sea. Weeks with considerable new ice formation are highlighted with vertical shading (winter events—yellow shading, spring events—orange shading). Based on these events, there are four periods defined for further analysis.

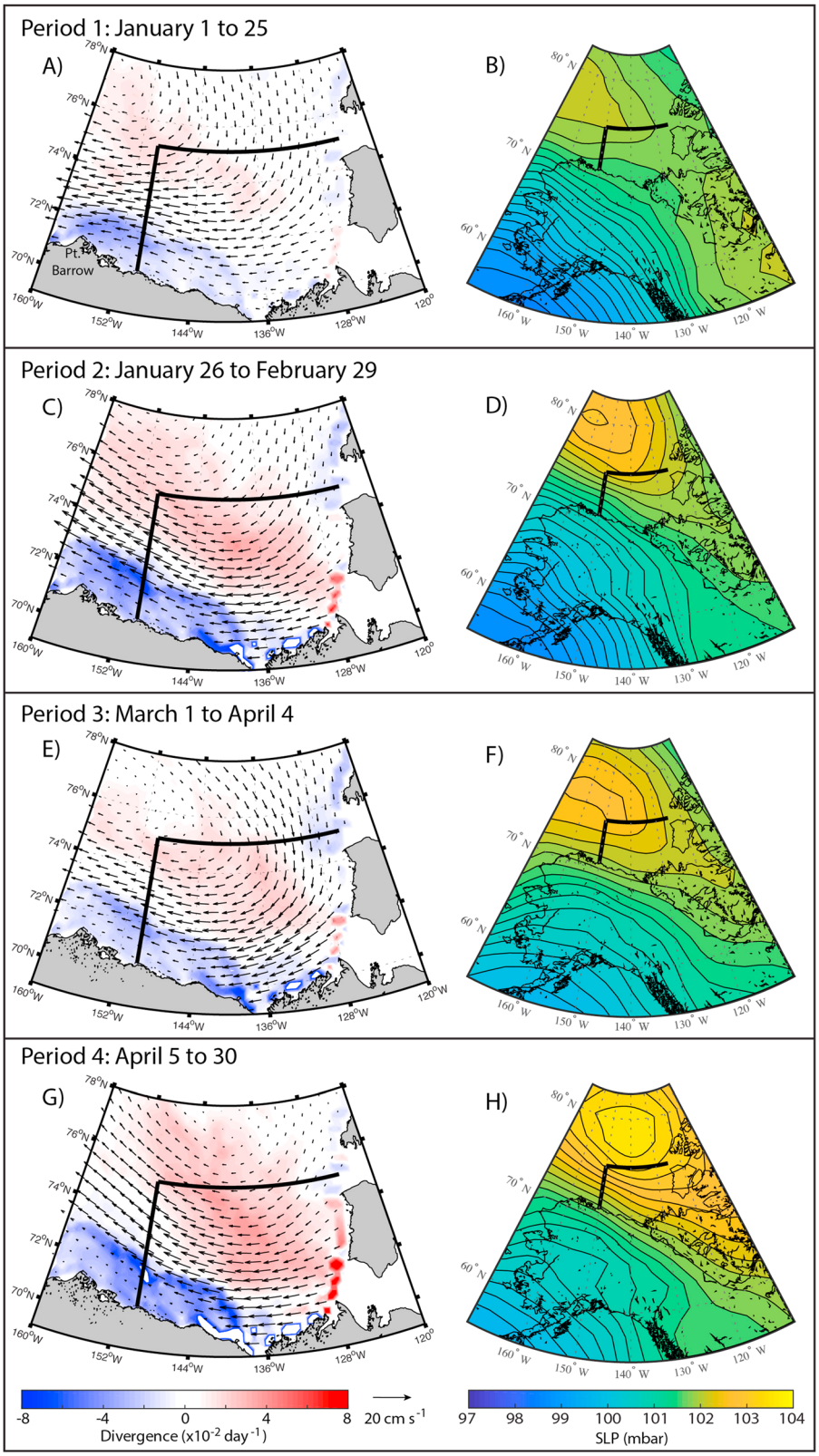


**Figure 6.** Mean fields of ice drift and sea ice divergence (left column), and sea level pressure patterns (right column) over the Beaufort Sea during the four periods in seasonal ice formation outlined in Figure 5. The thick black lines denote the northern and western gates of the Beaufort Sea, as presented in Figure 1. Note that for clarity only every second ice drift vector is shown.

(Figure 6). This restricts the formation of new ice to the eastern Beaufort Sea (Figure 3), but due to the anticyclonic Beaufort Gyre, these inclusions of anomalous thin ice types were advected westward and spread into the western Beaufort Sea (Figure 3; Daily SMOS data—not presented).

Overall, from January to April 2016 there was a strong SLP gradient across the Beaufort Sea from a pronounced Beaufort High to the Aleutian Low in the Gulf of Alaska (Figure 7a). This SLP gradient drove enhanced westward sea ice drift that created a negative net sea ice balance and caused the ice cover to diverge, opening up vast areas of open water where new ice subsequently formed (Figure 7b). Compared to the 1979-2008 climatology, the ice cover was much more mobile and divergent during 2016 (Figure 7d). In terms of the SLP pattern, 2016 was typical spatially, but the magnitude of the gradient across the Beaufort was greater than the climatology. While SLP varies interannually, previous years with similar SLP gradients do not show the same response in terms of ice export and divergence (Figure S1). Hence, decadal preconditioning toward a younger, thinner, more mobile ice cover facilitated the export and divergence observed during 2016.

### 3.3. Ice Thickness Anomalies

While new ice quickly forms within areas of open water during winter and maintains a highly concentrated ice cover, it changes the physical properties of the ice cover and leaves a lasting imprint that can be traced through subsequent observations of ice thickness. Following the initial increase in ice volume during fall freeze-up, the regional ice volume reached 400 $km^3$ by December 2015 and increased slightly to 467 $km^3$ by late-January (Figure 8). Based on the previous 5 years of CS2/SMOS observations, sea ice volume in January 2016 was similar to 2011, 2012, and 2013, while January 2014 and 2015 had greater ice volumes that can be traced back to increased ice volumes during October (Figure 8) as a result of relatively high sea ice extents during the previous September minima (Figure 1). Spatially, January 2016 was typical of the previous 5 years and the longer historical context from ice charts (Galley et al., 2016), with thin ice near the flaw lead in the south and thicker ice in the northwest where MYI is advected into the region (Figure 9). However, sea ice export and new ice formation during Period 2 led to a decrease in ice volume during late-January and early February at a time of year when ice volume typically increases within the Beaufort (Figure 8). The reduction and plateau of ice volume around 425 $km^3$ was due to negative ice thickness anomalies of up to 1 m that developed throughout the Eastern Beaufort Sea (Figure 9). By the end of Period 2 and start of March the regional ice volume was 418 $km^3$, only 21 $km^3$ greater than it was at the start of December over a period when the ice volume had on average increased by 252 $km^3$. Even during 2013 when ice volume increased slowly during winter, there was still a 116-$km^3$ increase in volume over this period. Calm conditions and reduced ice export during Period 3 allowed the regional ice cover to thicken during March, reducing the ice thickness anomalies and allowing ice volume to increase to 555 $km^3$ by the start of April. However, the return of strong atmospheric forcing and ice export during Period 4 once again caused divergence the ice cover, creating ice thickness anomalies of up to −1 m in the western Beaufort Sea (Figure 9) and reducing regional ice volume (Figure 8). Ultimately, the final regional ice volume from CS2/SMOS was 200 $km^3$ (−30%) below the 2011-2015 mean, leaving an ice cover that was inherently less resilient to summer melt and more responsive to atmospheric forcing that in turn fostered the dynamically driven breakup of the ice cover during Period 4.

### 3.4. Spring Breakup and Summer Ice Loss

The regional loss of sea ice within the Beaufort Sea from the start of spring breakup to the September minimum represents a balance of local sea ice melt and sea ice transport, with the latter either exacerbating ice loss through ice export or diminishing ice loss through import. Historically, sea ice area within the Beaufort Sea remained high through April and May and did not start to decline considerably until June (Figure 10). Years of previous sea ice minima in the Beaufort Sea have been characterized by premature breakup of the ice cover during May that increased solar absorption and enhanced ice melt through the ice albedo feedback. During 2016, the regional ice cover broke-up on 11 April, 7 weeks earlier than the 1979–2008 mean breakup date of 22 May. By 2 May the regional sea ice area had dropped to 300,000 $km^2$, which was several weeks prior to previous sea ice minima (23 May 1998, 5 June 2008, and 8 June 2012) and almost 2 months prior to the climatological mean of 1 July (Figure 10). The regional sea ice area was at a 38-year minimum throughout May 2016 but plateaued around 200,000 $km^2$ during early June and fell in line with the three

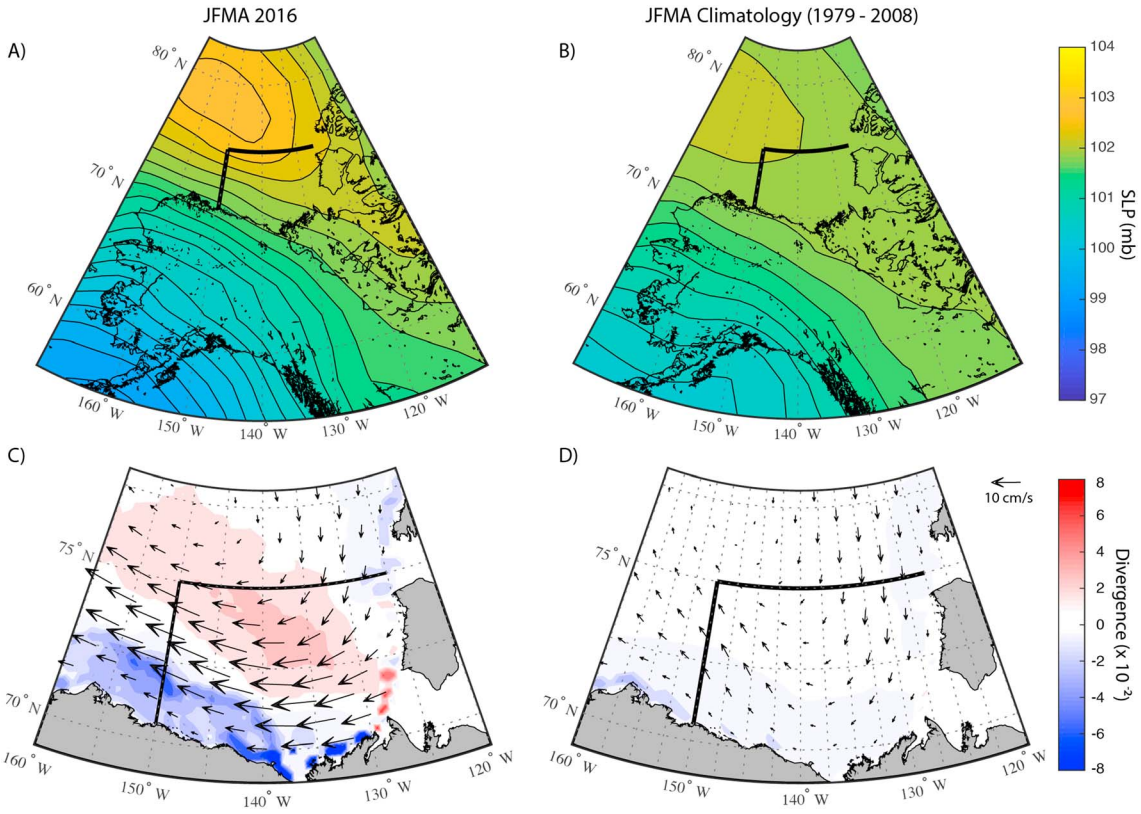


**Figure 7.** Mean fields of (a and b) sea level pressure (SLP) and (c and d) ice drift and divergence over the Beaufort Sea from January to April (JFMA) for 2016 (a and c) and the 1979-2008 climatology (column and d). SLP contours are at 0.2-mb intervals. The thick black lines on each panel denote the western and northern perimeter of the Beaufort Sea. Every fourth ice drift vector is presented for clarity.

previous sea ice minima. Subsequently, sea ice area declined during late June and July until the region was ice-free by mid-August. Between the regional breakup on 11 April and mid-September, there was 425,000 km$^2$ of sea ice lost from the Beaufort Sea. From the daily time series of ice flux across the northern and western gates it is clear that ice export across both gates contributed to the breakup of the ice cover during late-April. Overall between the date of regional breakup and the mid-September sea ice minimum, there was a net export of 26,140 km$^2$, meaning that 396,660 km$^2$ (i.e., 15 times more ice)

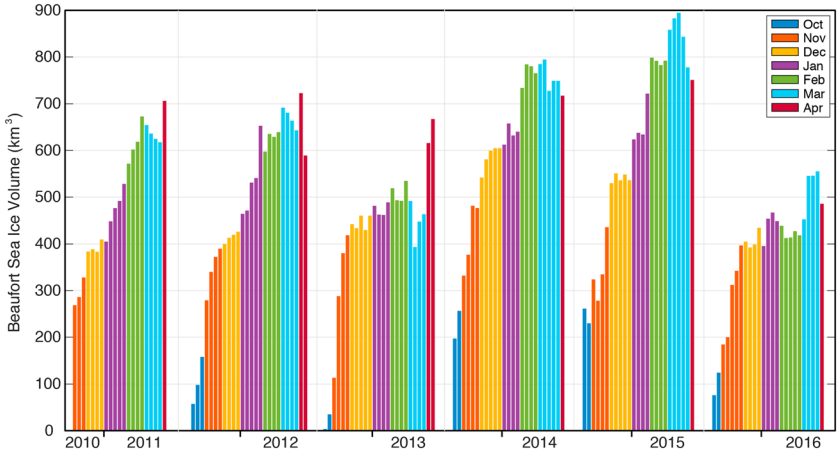


**Figure 8.** Weekly sea ice volume (km$^3$) in the Beaufort Sea from October to April for each year of the Cryosat-2 record (2011–2016).

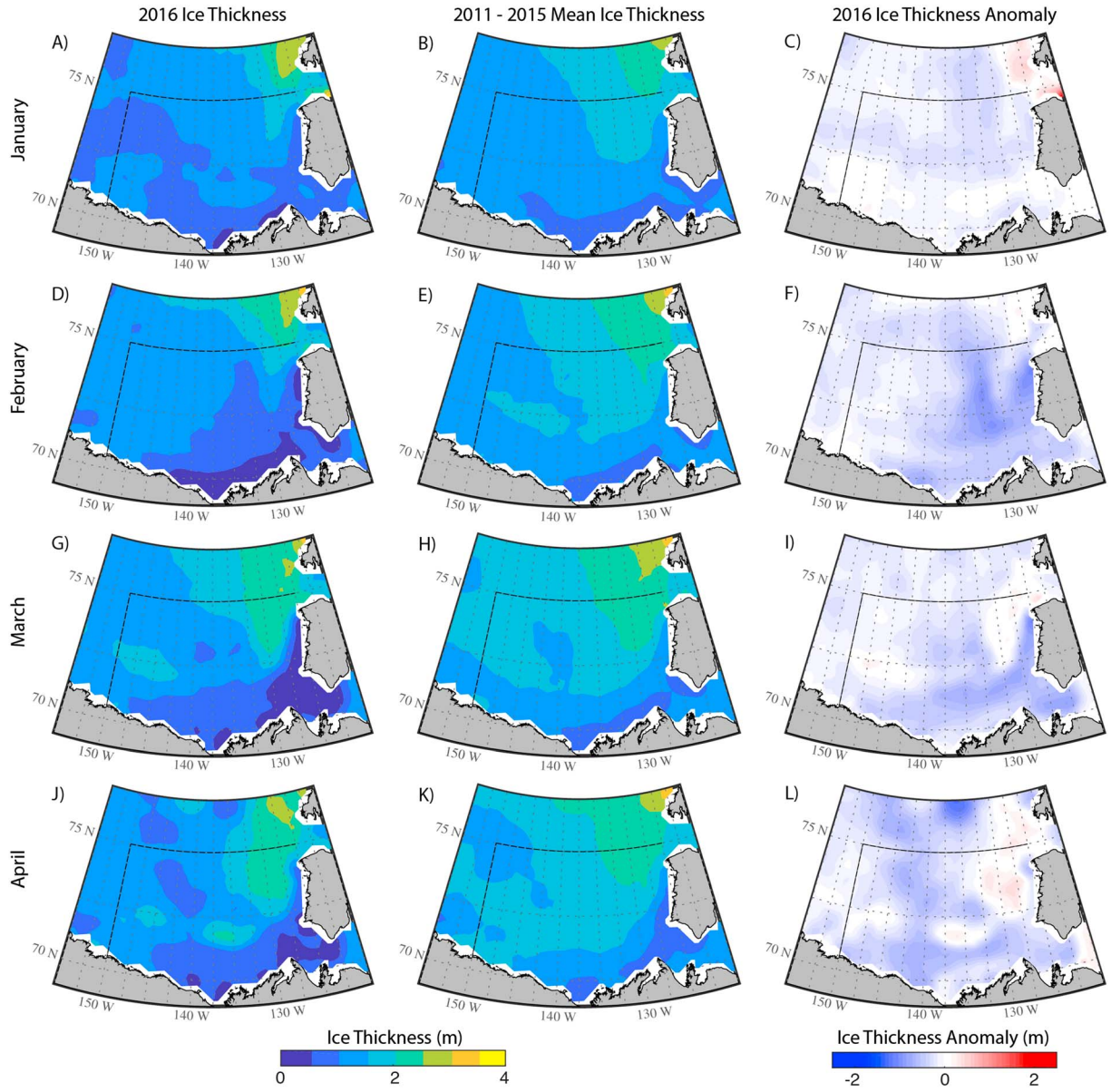


**Figure 9.** Ice thickness in the Beaufort Sea from January to April during (a, d, g, and j) 2016, (b, e, h, and k) the 2011–2015 mean, and (c, f, i, and l) the 2016 ice thickness anomalies (right column).

melted locally. The deviation between sea ice area lost and net sea ice transport began in late-April and corresponds with a rise in air temperature (Figure 10d) and the onset of daily solar absorption through areas of open water (Figure 10e). During May northern import offset western export, yet the regional sea ice area declined rapidly. Increasing solar irradiance and a +2.2°C anomaly in the regional monthly air temperature (Figure 10) likely led to the quick loss of thin ice types within the ice cover (Figure 2). By the end of May there was a 400% anomaly in cumulative solar absorption through areas of open water, strengthening the regional ice-albedo feedback. From June to August air temperatures returned to climatological values and there was a net sea ice import; however, considerable solar energy had been absorbed by the upper ocean and the fractured nature of the ice cover did not confine solar heating to the periphery of the ice cover but instead allowed heating to occur within pack ice (Figure 4a). With an accelerated ice-albedo feedback and a fractured, anomalously thin ice cover, the regional sea ice area declined quickly and was completely lost by mid-August.

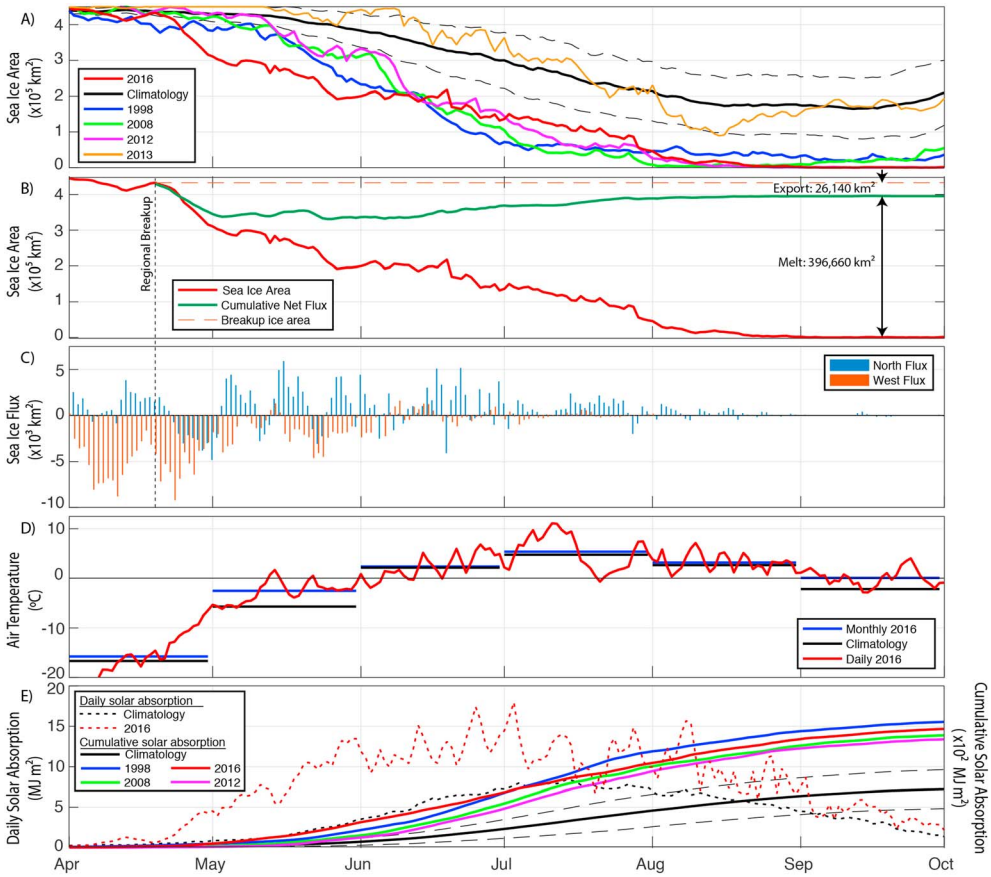


**Figure 10.** The seasonal time series from April to September of (a) daily regional sea ice area ($km^2$) for the 4 years of regional sea ice minima and the 1979–2006 climatology ± 1 standard deviation, (b) daily net ice flux ($km^2$)across the north (blue) and west (red) gates, (c) daily sea ice area during 2016 and the daily cumulative ice transport from the day of regional breakup (regional sea ice concentration < 95%, 22 April), and (d) regional mean air temperature—daily for 2016 (red), monthly for 2016 (blue), and the monthly 1979–2006 climatology (black). (e) daily ($W/m^2$) and cumulative ($MJ/m^2$) solar absorption through areas of open water within the Beaufort Sea with the daily climatology (black dots) and cumulative climatology (solid black) ± 1 standard deviation (dash black).

Focusing on the contribution of export and melt to summer ice loss within the Beaufort Sea, we find that during the 38-year satellite record, local ice melt was greatest during 2016 (Figure 11). Of the regional sea ice area at the time of breakup, 93.8% melted locally. Assuming that ice volume was equally exported (Figure 8), 455.5 $km^3$ of sea ice melted in the Beaufort Sea during 2016. Assuming an ice density of 900 $kg/m^3$ and the latent heat of fusion of fresh ice to be 0.335 MJ/kg, $1.37 \times 10^{14}$ MJ was required to melt this volume of ice. Our calculations indicate that sufficient solar energy was absorbed through areas of open water (Figure 10e; regional total $6.38 \times 10^{14}$ MJ) to satisfy this requirement and melt the end of winter ice cover 4 times over. Of course not all heat is directed toward ice melt and excess energy heats the upper ocean, delaying freeze-up and leading to the formation of a near-surface temperature maximum that can limit thermodynamic growth during the following winter (i.e., Timmermans, 2015). Again, this calculation of solar absorption is a conservative estimate, as it does not consider solar energy transmitted through ice, of which the vast areas of young ice, that had likely accumulated only a thin snow cover and therefore had a low albedo (Ehn et al., 2007), would have allowed considerable transmission and contributed to greater warming in the upper ocean.

## 4. Discussion

### 4.1. In Situ Observations of the Preconditioned Ice Cover

Prevalence of thin sea ice within the Beaufort ice cover at the end of winter 2016 was confirmed by aerial ice thickness surveys in April 2016 (Haas et al., 2016). Ice thickness distributions from both the MYI and FYI

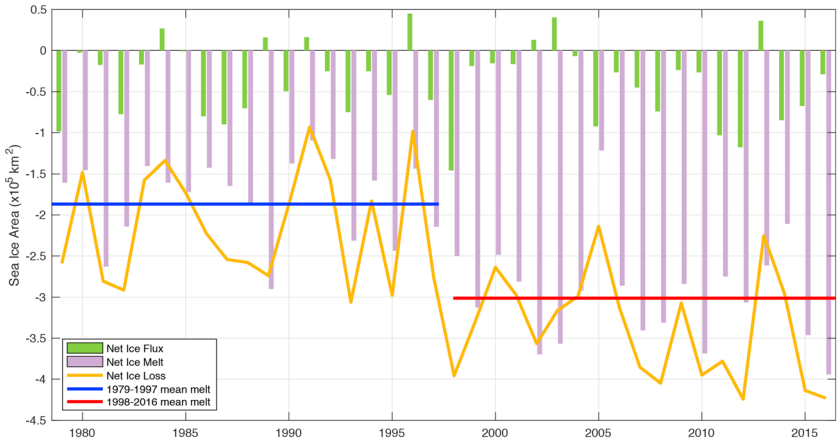


**Figure 11.** Annual loss of sea ice in the Beaufort Sea from the date of date of regional breakup (<95% regional sea ice concentration) to 15 September (yellow), separated into the dynamic (ice transport, green) and thermodynamic (ice melt, purple) components of ice loss. The 1979–1997 and 1998–2016 mean amount of ice melt is also presented.

regions of the Beaufort Sea reveal a thin ice pack compared to previous years, with lower modal thicknesses and reduced presence of thicker ice in the right tail of the distributions. But perhaps most importantly the survey highlighted the presence of vast areas of thin ice within the fractured MYI cover and documented the premature presence of open water within a very thin FYI cover in the southern Beaufort Sea. While Haas et al. (2016) suggest that this predisposed the Beaufort to a large ice loss in 2016, within this study, we have identified the process that created this thin fractured ice cover, provided regional context beyond the aerial survey, and showed how the conditioned ice cover broke up and declined rapidly during summer.

### 4.2. JFMA Ice Export Variability

As a marginal sea within the Beaufort Gyre, the Beaufort Sea is heavily influenced by the transport of sea ice. Generally, sea ice is exported to the west and imported from the north, though typically more ice is exported than imported (Petty et al., 2016) and the Beaufort experiences a net-negative sea ice budget (Figure 12). From 1979 to 2008 there was an average cumulative export of 68,250 $km^2$ out of the Beaufort Sea from January to April (Figure 12). There were only 2 years of net ice import (1989: 29,230 $km^2$ and 1990: 87,280 $km^2$; Figure 12), while the 3 years of greatest net export correspond to three of the four regional September sea ice minima (2016: −338,000 $km^2$, 1998: −280,300 $km^2$, and 2008: −220,400 $km^2$; Figure 12). However, there is considerable variability in ice transport (Figure 12), with periods of rapid sea ice export (e.g., late-February to early-March 2013 and April 2016), notable sea ice import (e.g., April 2013 and January 2012), and prolonged periods of negligible ice transport (e.g., February to March 2012). This variability is reflective of ice transport across both the northern and western gates (Figure 13). For example, periods of rapid net ice export are typically characterized by enhanced western ice export that can either be partially offset by northern ice import (e.g., March 2013; Figure 13c), aligned with negligible northern transport (e.g., April 2016; Figure 13d), or enhanced by northern export (e.g., March 1998; Figure 13c).

The record export of 338,000 $km^2$ during 2016 was over 5 times greater than the climatological mean export of 68,250 $km^2$ and was the result of the largest monthly exports on record during February and April. The net export of 146,820 $km^2$ during April 2016 is the single largest monthly export from January to April during the 38-year study period, while the export of 110,780 $km^2$ during February 2016 is the third largest (Figure 13). Although the western export was actually greater during February 2016, so to was northern import, which offset some of the western ice export. Western ice export was also high during March 2016, but northern import balanced it out and limited new ice formation during March (Figures 2 and 5).

While sea ice export was episodic during 2016, it was persistent during 1998 as a result of persistent southerly and easterly winds (Maslanik et al., 1999) that enhanced western ice export, and either limited northern import or drove northern export (Figures 13 and S1; Kwok, 2006a). During winter 1998, there was a net northern export of 19,500 $km^2$ compared to a climatological northern import of 42,400 $km^2$. This led to

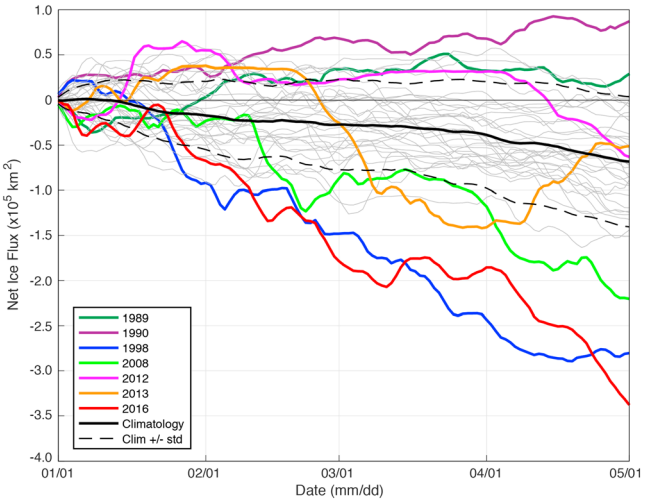


**Figure 12.** Cumulative sea ice transport from January to April for each year from 1979 to 2016. The 1979–2008 climatology is presented in black along with ±1 standard deviation. Years of sea ice minima (1998, 2008, 2012, and 2016) are presented along with the two years of cumulative net ice import (1989, 1990) and 2013.

the lowest end of winter regional concentration of MYI (Figure 2e), an anomalously thin ice cover in the southeastern Beaufort Sea (Melling et al., 2005) and the continual formation of new ice within the region. However, unlike 2016, the ice cover was only slightly divergent from January to April 1998 (Figure 13) and moved coherently, remaining intact and limiting new ice formation to the flaw leads in the southern Beaufort Sea (CIS ice charts—not shown). As a result, the MYI cover shifted northward, and even though the FYI-dominated southern Beaufort Sea prematurely broke up and melted out during May and June (Figure 10), the MYI consolidated during this time and was therefore able to retard summer melt and maintain a partial ice cover throughout summer 1998 (Figure 10). Additionally, the MYI cover of 1998 was likely thicker than the MYI cover that has occupied the Beaufort Sea during recent years (e.g., Barber et al., 2009), making it more resilient to summer melt and the ice albedo feedback during a year of enhanced solar heating (Figure 10).

The anomalous forcing of 1998 and resultant flushing of MYI from the Beaufort caused a shift in the composition of the Beaufort ice pack toward enhanced seasonal ice coverage (Hutchings & Rigor, 2012) that predisposed the region to enhanced summer melt. This is obvious in the time

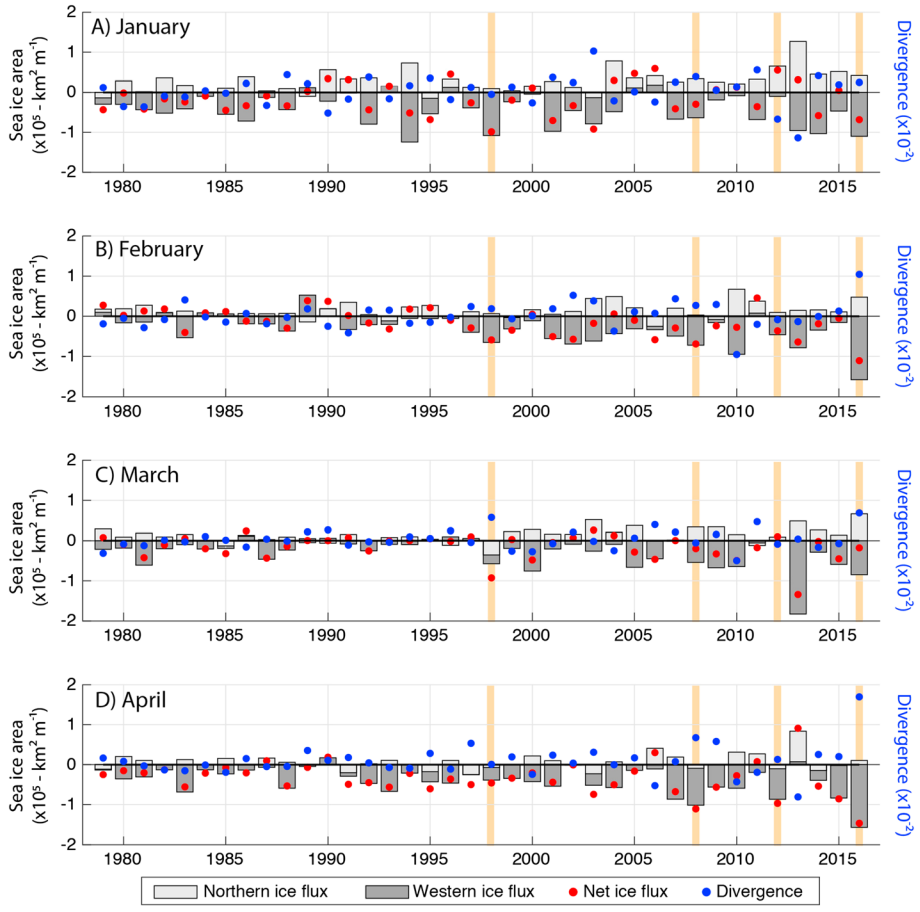


**Figure 13.** The monthly time series of the northern ice flux (km$^2$, light grey), western ice flux (km$^2$, grey), net ice flux (km$^2$, red), and cumulative divergence (x10, blue) from January to April between 1979 and 2016. Positive values indicate sea ice import into the Beaufort or divergent ice motion. The four sea ice minima are highlighted with orange shading.

series of September sea ice area (Figure 1), but this change also affected the dynamic properties of the ice cover and resulted in an increase in ice transport during February, March, and April between the pre-1998 and post-1998 periods (Figure 13). Historically, ice transport reached its annual minimum during this period, as the cold, thick, mechanically strong ice cover would have considerable internal stresses that would dampen external forcing. However, since 1998 the winter ice cover has been more mobile [i.e., Petty et al., 2016] and ice transport across both the northern and western gates has increased (Figure 13).

The largest monthly western ice export (182,750 $km^2$) of the 38-year study period occurred during March 2013. This event was over 160,000 $km^2$ greater than the climatological March export of 21,118 $km^2$. While the record export was partially offset by northern import (48,802 $km^2$), there was a net monthly export of 133,950 $km^2$ (Figure 13). In a manner similar to the two periods of intense ice export during 2016, this event led to considerable new ice formation (Figure 2e) and reduced the regional ice volume (Figure 8). The increased export was the result of a series of storms that initiated a large fracture event in the Chukchi Sea during January, which gradually spread throughout the Beaufort Sea during February and March (Beitsch et al., 2014; NSIDC, 2013). The unusual fracturing event was attributed to the long-term transition toward a seasonal ice cover (NASA Earth Observatory, 2013), which is inherently weaker and therefore more responsive to atmospheric forcing. The ice cover within the Chukchi Sea during winter 2013 was especially thin because during the previous summer, the entire Beaufort Sea had melted out (Babb et al., 2016), leaving no remnant thick FYI or MYI to be advected into the Chukchi Sea during autumn 2012 or winter 2013 (Howell et al., 2016). Furthermore, MYI replenishment within the Beaufort Sea was limited during autumn 2012 and winter 2013, because the MYI pack was confined to a narrow band along the CAA (Howell et al., 2016). While the regional MYI concentration did increase from January to March 2013, it was still at a record low (Figure 2e), making the predominantly seasonal ice cover susceptible to this fracture event. Following this event, the now younger and thinner ice cover was theoretically preconditioned for premature breakup and rapid melt during summer, just like in 2016. However, during April, the largest net import of the 38-year record (91,131 $km^2$) occurred as a result of sea ice import across the northern (83,857 $km^2$) and western (7,274 $km^2$) gates. This caused the ice cover to converge (Figure 13) and increased the regional ice volume through dynamic deformation (Figure 8). Ultimately breakup during spring 2013 was delayed past the climatological mean (Figure 10a), which delayed solar absorption and limited the ice albedo feedback. While a reduced ice albedo feedback theoretically would have limited bottom and lateral melt of the ice cover, cool air temperatures, and elevated albedos reduced surface melt during summer 2013 (Kwok, 2018). At the same time, convergence against the CAA (Kwok, 2015) imported ice during summer (Figure 11) and consolidated MYI within the Eastern Beaufort Sea (CIS ice charts—not shown). Collectively, these thermodynamic and dynamic processes limited sea ice loss during 2013 and led to the recovery of the regional sea ice cover to its third highest September sea ice area since 1998. Retention of sea ice within the Beaufort Sea during summer 2013 allowed MYI and thick FYI to persist, leading to a 10-year peak in MYI concentration in January 2014 (Figure 2b) and a thicker ice cover (Figure 8).

From Figure 12 it is clear that enhanced sea ice export played a role in preconditioning the Beaufort ice cover prior to the September sea ice minima of 1998, 2008 and 2016. But what about 2012? Previous work in Babb et al. (2016) attributed the complete loss of the Beaufort ice cover during September 2012 to a combination of long-term preconditioning and episodic events during the summer of 2012. Specifically, in terms of seasonal preconditioning of the ice cover through winter ice export, we can see that there was in fact a net import of 28,823 $km^2$ from January to March 2012, which limited the formation of new ice (Figure 2), and led to a regional ice volume of 710 $km^3$ by April (Figure 8). However, a large western export (86,715 $km^2$) and subtle northern export (10,277 $km^2$) during April (net export of 96,992 $km^2$; Figure 13d) drove the premature breakup that contributed to rapid ice loss during May, June, and July 2012 (Figure 10).

While various dynamic and thermodynamic processes dictate how the regional ice cover evolves during the melt season, there is an inherent relationship between the state of the ice cover at the start and end of the melt season. Provided that ice transport during winter influences the state of the ice cover at the end of winter or start of the melt season, there is an intuitive relationship between winter ice transport and September ice conditions in the Beaufort Sea. Historically, the MYI-dominated ice cover of the Beaufort Sea showed no relationship between January to April ice export and September sea ice area (Figure 14, blue). However

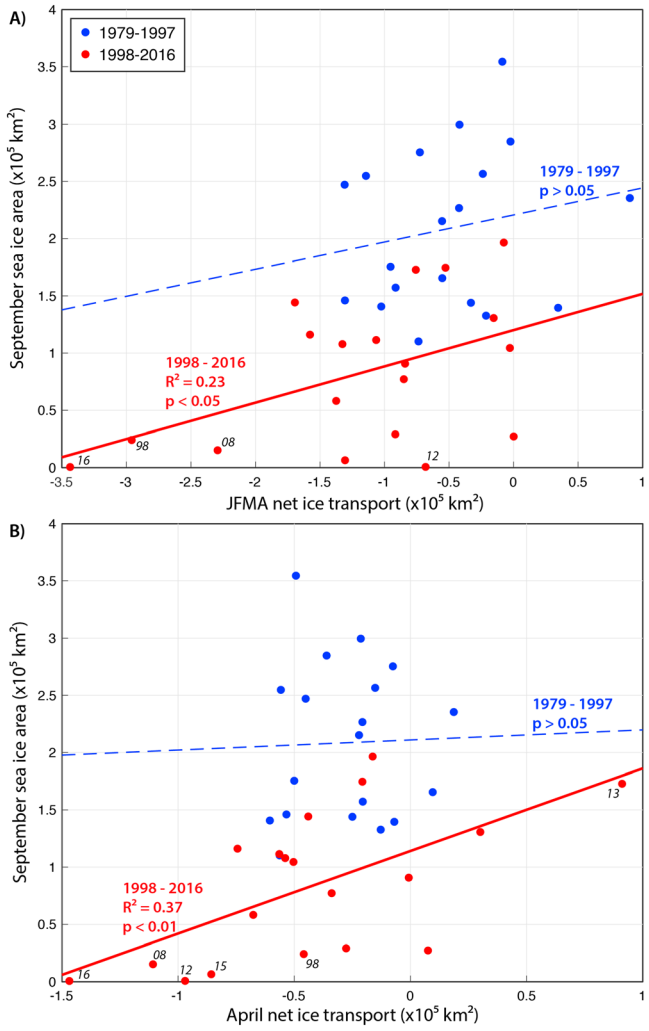


**Figure 14.** Scatterplots of the (a) net January to April ice transport (km$^2$) and (b) net April ice transport (km$^2$) against the mean September sea ice area in the Beaufort Sea (km$^2$). Data are separated around 1998, with 1979–1997 presented in blue, and 1998–2016 in red. The correlation coefficient ($R^2$) and associated $p$-value are presented for each. The four sea ice minima and other notable years are labeled for reference.

following 1998, there has been a statistically significant relationship between January to April ice export and September sea ice area (Figure 14, red; $R^2 = 0.22$, $p < 0.05$), indicating winter ice export is an effective conditioning mechanism that promotes summer ice loss. The relationship indicates that for every 100,000 km$^2$ of net sea ice export from the Beaufort Sea between January and April, the September sea ice area declines by 31,720 ± 5,760 km$^2$. Variability about this relationship is driven by summer conditions that cannot be forecast and complicate seasonal predictions (Petty et al., 2017; Serreze, Stroeve et al., 2016), such as the Great Arctic Cyclone of 2012 that accelerated ice loss in the Beaufort Sea or convergence against the CAA during 2013 that retained sea ice within the Beaufort during summer (Howell et al., 2016). Ice transport during April is particularly important as the first areas of open water in the Beaufort are created dynamically (Steele et al., 2015) and initiate the ice-albedo feedback that accelerates summer melt. Historically, the relatively quiescent April ice cover (Figure 13d) had no relationship to September sea ice area. However, following 1998, there has been a statistically significant relationship that explains 37% of the variance in regional September sea ice area and indicates that for every 100,000 km$^2$ of net sea ice export during April, there is a reduction of 72,110 ± 5,200 km$^2$ in the regional September sea ice area (Figure 14b; $R^2 = 0.37$, $p < 0.01$). Enhanced ice export during April 2016 was preceded by ice export during February and March, whereas enhanced ice export during 2012 and 2015 was not (Figure 14b). This indicates that early winter preconditioning can amplify summer melt, but preconditioning immediately prior to melt onset in April can enhance summer melt on its own. Conversely, ice import during April 2013 essentially undid the seasonal preconditioning of February and March, delaying breakup of the ice cover and limiting ice loss during summer 2013 (Figure 14b).

### 4.3. Summer Transport and Melt

The regional loss of sea ice during the melt season reflects both dynamic and thermodynamic processes. During 2016, sea ice loss was predominantly driven by local ice melt and while the same amount of ice was lost during 2012, ice export contributed to a much greater extent (Figure 11). The largest cumulative summer export of the 38-year time series occurred during 1998 (134,800 km$^2$) and permanently transitioned the Beaufort toward a younger ice cover that was more prone to summer melt (Hutchings & Rigor, 2012). As a result, the mean amount of ice lost to summer melt increased from 183,160 km$^2$ between 1979 and 1997 to 301,050 km$^2$ between 1998 and 2016 (Figure 11). The increase in average regional ice melt of 118,000 km$^2$ explains 92% of the 128,000 km$^2$ change in September sea ice area between these two periods (Figure 1b) and indicates that summer thermodynamic melt is driving sea ice loss in the Beaufort Sea. Over the 38-year time series, sea ice is typically exported from the Beaufort during the melt season; however, there was a net sea ice import during seven summers. Ice import is typically associated with years of high September ice areas (Figure 1b; e.g., 1991, 1996 and 2013). Ice import during 1996 and 2013 was associated with negative SLP anomalies over the Arctic Ocean and larger scale convergence of the Arctic ice pack against the CAA (Kwok, 2015; Serreze, Crawford et al., 2016), which allows the ice cover to coalesce and persist through summer. During recent years, the transport component of summer ice loss has been changing as greater ice melt in the pacific sector and northward retreat of the ice cover has left the western gate ice-free for prolonged periods during summer (Howell et al., 2016). Therefore, in terms of ice flux the increase anticipated through an increasingly mobile ice cover may be offset by reductions in sea ice concentration and the retreat of the ice edge.

### 4.4. Continued MYI Loss in the Beaufort Sea

The continual transition of the Arctic ice pack from one dominated by MYI to one comprised of mostly FYI ice has major implications for the physical properties of the ice pack and its resilience to summer melt. Historically, the Arctic ice pack retained the oldest ice types through recirculation within the Beaufort Gyre. However, increased summer melt in the Beaufort Sea during recent years has precluded MYI from surviving its southern pass through the Beaufort Sea and, following Maslanik et al. (2007), essentially severed the previously continuous clockwise journey of MYI. This has contributed to the pan-Arctic decline in MYI, as younger ice is both recirculated within the Beaufort Gyre (Hutchings & Rigor, 2012) and advected to other areas of the Arctic through the Transpolar Drift Stream (e.g., Haas et al., 2011). Galley et al. (2013, 2016)) showed that MYI concentration within the Beaufort Sea has significantly declined during both winter and summer, with the greatest trends occurring during summer. This significant negative trend has now been punctuated by the complete loss of the end of winter MYI cover during summer during three of the last eight years (2010— Stroeve et al., 2011, 2012–Babb et al., 2016, and 2016–this study). An overall trend toward reduced MYI concentration within the Beaufort, punctuated by the complete loss of the MYI pack during several recent years, has greatly reduced the probability of MYI staying intact as it is advected through the Beaufort Sea downstream to the Chukchi and East Siberian Seas. Both of these marginal seas have seen a reduction in MYI area during the observational record and have more recently been left completely free of MYI by the end of winter (Maslanik et al., 2011). While Serreze, Crawford et al. (2016) found that the MYI fraction during winter and spring was not correlated with breakup dates in the Chukchi Sea, the reduced presence of MYI within the Chukchi does intuitively predispose the region to greater and faster loss of sea ice during summer as a thinner ice pack is less resilient to the warm pacific water flowing in through the Bering Strait and the subsequent ice albedo feedback.

Within the Beaufort Sea, MYI loss is caught in a positive feedback, whereby the recirculation of younger ice back into the Beaufort through the Beaufort Gyre (Hutchings & Rigor, 2012) promotes further reduction of the mechanical strength of the winter ice pack. This creates a more mobile ice pack that is prone to enhanced ice export during winter (Figure 13), which in turn increases the presence of younger and thinner ice types by the end of winter. A younger and thinner ice cover is prone to breakup earlier, thereby exposing greater areas of open water while solar radiation is high, and initiating the ice albedo feedback that drives increased ice melt and the further loss of MYI. This process threatens to accelerate summer sea ice loss within the Beaufort, which will render it ice-free more often and contribute to the continued upstream progression of MYI loss within the Beaufort Gyre.

### 4.5. Dynamic Preconditioning—From the Beaufort to the Central Arctic

The role of enhanced winter ice export preconditioning a regional ice cover for increased summer melt is not limited to the Beaufort Sea. In the Laptev Sea, Itkin and Krumpen (2017) found that offshore winds during winter increase sea ice export and foster a thinner end of winter ice cover that then retreats further during summer. Now that marginal seas are susceptible to atmospherically driven divergence, dynamic preconditioning is clearly able to enhance summer ice melt; but what about the central Arctic Ocean? Historically, the central Arctic has contained the thickest and oldest ice types, which are typically compressed against northern Greenland and the western flank of the Canadian Arctic Archipelago (Kwok, 2015). However, like much of the Arctic, this region has experienced a reduction in ice thickness (Kwok, 2018) that has reduced internal stress, increased floe mobility, and theoretically increased the ice covers capability of responding to atmospheric forcing. During winter 2018, an anomalous period of sustained southerly winds advected the ice cover north of Greenland offshore, exposing a vast area of open water adjacent to the coast (Moore et al., 2018b; NSIDC, 2018a) and subsequently creating a large area of thin ice (Daily SMOS data—not shown). During the ensuing summer, southerly winds once again opened the same area, which is unusual and was attributed to the broken-up, anomalously thin ice cover, which had occupied the area (NSIDC, 2018b). Regardless of the 6 months that separated these two events, they show that dynamic preconditioning during winter exposes the summer ice cover, enabling the formation of open water in regions characteristically ice-covered in summer. Specifically, it highlights that processes critical in producing ice-free conditions in both the Beaufort and Laptev Seas can be effective in triggering the ice-albedo feedback within the central Arctic Ocean. Dynamic preconditioning of the winter ice cover

for rapid summer melt may become increasingly important as the greater Arctic ice pack becomes increasingly seasonal and mobile.

## 5. Conclusions

For the second time in 5 years, and the second time in the entire observational record, the Beaufort Sea became ice-free during September 2016. Over the 38-year satellite record there is a significant negative trend of −5,236 $km^2$/year in September sea ice area within the Beaufort Sea. However, over the last decade this trend has been amplified as the region has experienced eight of its nine lowest September sea ice areas and been left completely ice-free twice. Since 1998 the regional ice cover of the Beaufort Sea has transitioned from one dominated by MYI to a more seasonal ice cover that is not only more prone to summer melt but also increasingly dynamic and responsive to atmospheric forcing.

Historically, during winter, the Beaufort ice cover has been comprised of thick MYI that kept the ice cover relatively quiescent and limited the dynamic formation of open water to the coastal flaw lead system. However, in 2016, the ice cover was much more dynamic, creating vast areas of open water where new ice formed and conditioned the ice cover toward younger and thinner ice types at the start of the melt season. While the thickness of the Beaufort ice cover during January 2016 was typical of the previous 5 years, enhanced sea ice export during February 2016 caused the ice cover to diverge, exposing vast areas of open water where new ice subsequently formed and created negative ice thickness anomalies. By mid-March, roughly, one third of the Beaufort ice cover was comprised of thin ice types, whereas historically, during March, 94% of the ice cover was comprised of either thick FYI or MYI. During April, another period of enhanced export amplified the negative ice thickness anomalies, causing the regional sea ice volume to fall 30% below the previous 5-year mean, and leading to the premature breakup of the ice cover. The preconditioned ice cover broke up 7 weeks prior to the climatological timing, but areas of open water were not limited to the southern Beaufort Sea as they typically are early in the melt season. Instead vast areas of open water formed within the ice pack, allowing the ice-albedo feedback to drive rapid melt during May and preferentially melt thin ice types. This created a heavily fractured and dispersed ice cover that completely melted out during August.

Overall sea ice export from January to April 2016 was the greatest of the 38-year satellite record and over 5 times the climatology. In fact sea ice export from January to April has been greatest prior to the regional sea ice minima of 1998, 2008, and 2016, while a large export during April 2012 contributed to the first instance of an ice-free Beaufort Sea. While enhanced ice export can precondition the ice cover, ice import can do the opposite. The largest monthly export of the satellite record occurred during March 2013 and preconditioned the ice cover toward younger and thinner ice types, however ice import and convergent ice drift during April negated the preconditioning, delaying breakup and contributing to the highest September sea ice area of the last decade. Overall, net sea ice transport from January to April, and during April, by itself have been significantly correlated with the regional September sea ice area since 1998, explaining between one quarter and one third of the variance and offering the potential for forecasting sea ice conditions within the Beaufort during summer. Clearly sea ice transport is a key process for the Beaufort Sea ice cover, especially as MYI is caught in a negative feedback mechanism and the increasingly seasonal ice cover becomes more responsive to atmospheric forcing. Continued trends toward increased summer sea ice loss, specifically MYI loss, will promote more frequent occurrence of extreme ice-free conditions within the Beaufort Sea, and more broadly the Arctic Ocean as similar processes continue to drive it toward itself becoming ice-free within the not-too-distant future.

**Acknowledgments**
This work was supported by D. G. Barber's Canada Research Chair. D. G Babb, R. J Galley, and D.G. Barber are supported by the Natural Sciences and Engineering Research Council of Canada (NSERC). J. C. Landy is supported by the ESA Living Planet Fellowship: ESA/4000125582/18/I-NS (Arctic-SummIT). This work is a continuation of work that began during the Canadian Governments Beaufort Regional Environmental Assessment (BREA) with our colleague K. Hochheim. Thanks to Y. Lou from Environment Canada for sharing the Radarsat mosaics with us. Thanks to the Editor, S. Howell and one anonymous reviewer for their useful comments and suggestions. Thanks to A. Proshutinsky for coordinating this special issue on the Beaufort Gyre. This is a contribution to the Arctic Science Partnership (ASP, www.asp-net.org). CIS ice charts are available from the CIS (http://iceweb1.cis.ec.gc.ca). The Polar Pathfinder ice drift dataset is available from the NSIDC (https://nsidc.org/data/nsidc-0116/versions/3). The passive microwave NASA-Team sea ice concentration data are available from the NSIDC (https://nsidc.org/data/NSIDC-0051/versions/1). The NCEP reanalysis2 atmospheric fields are available from NOAA (https://www.esrl.noaa.gov/psd/data/gridded/data.ncep.reanalysis2.html). The ERA-interim atmospheric reanalysis fields are available from ECMWF (https://apps.ecmwf.int/datasets/data/interim-full-daily). The Cryosat-2/SMOS weekly fields of ice thickness area available from AWI *Meereisportal* (https://www.meereisportal.de/en.html).

## References

Agnew, T., & Howell, S. E. L. (2003). The use of operational ice charts for evaluating passive microwave ice concentration data. *Atmosphere-Ocean*, *41*(4), 317–331. https://doi.org/10.3137/ao.410405

Babb, D. G., Galley, R. J., Barber, D. G., & Rysgaard, S. (2016). Physical processes contributing to an ice free Beaufort Sea during September 2012. *Journal of Geophysical Research: Oceans*, *121*, 267–283. https://doi.org/10.1002/2015JC010756

Balmaseda, M. A., & Mogensen, K. (2010). Evaluation of ERA-Interimforcing fluxes from an ocean perspective. *European Center for Medium-range Weather Forecasts (ECMWF)*, *ERA Rep. Ser. 6*. Shinfield Park, Reading.

Barber, D. G., Galley, R., Asplin, M. G., de Abreu, R., Warner, K. A., Pućko, M., et al. (2009). Perennial pack ice in the southern Beaufort Sea was not as it appeared in the summer of 2009. *Geophysical Research Letters*, *36*, L24501. https://doi.org/10.1029/2009GL041434

Barber, D. G., & Hanesiak, J. M. (2004). Meteorological forcing of sea ice concentrations in the southern Beaufort Sea over the period 1979 to 2000. *Journal of Geophysical Research*, *109*, C06014. https://doi.org/10.1029/2003JC002027

Beitsch, A., Kaleschke, L., & Kern, S. (2014). Investigating High-Resolution AMSR-2 Sea Ice Concentrations during the February 2013 Fracture Event in the Beaufort Sea. *Remote Sensing*, *6*, 3841–3856. https://doi.org/10.3390/rs6053841

Cavalieri, D., Parkinson, C., Gloersen, P., & Zwally, H. J. (1996, updated yearly). *Sea Ice Concentrations from Nimbus-7 SMMR and DMSP SSM/I-SSMIS Passive Microwave Data*. Boulder, CO: NASA DAAC at the National Snow and Ice Data Center.

Comiso, J. C., Parkinson, C. L., Gersten, R., & Stock, L. (2008). Accelerated decline in the Arctic sea ice cover. *Geophysical Research Letters*, *35*, L01703. https://doi.org/10.1029/2007GL031972

Cullather, R. I., Lim, Y.-K., Boisvert, L. N., Brucker, L., Lee, J. N., & Nowicki, S. M. J. (2016). Analysis of the warmest Arctic winter, 2015-2016. *Geophysical Research Letters*, *43*, 10,808–10,816. https://doi.org/10.1002/2016GL071228

Dee, D. P., Uppala, S. M., Simmons, A. J., Berrisford, P., Poli, P., Kobayashi, S., Andrae, U., et al. (2011). The ERA-Interim reanalysis: Configuration and performance of the dataassimilation system, *Quarterly Journal of the Royal Meteorological Society*, *137*, 553–597.

Eastwood, S. (2012). OSI SAF Sea Ice Product Manual, v3 .8 ed. MetNo, Norway.

Ehn, J. K., Hwang, B. J., Galley, R. J., & Barber, D. G. (2007). Investigations of newly formed sea ice in the Cape Bathurst polynya: 1. Structural, physical, and optical properties. *Journal of Geophysical Research*, *112*, C05002. https://doi.org/10.1029/2006JC003702

Fequet, D. (Ed.) (2005). *Manual of Standard Procedures for Observing and Reporting Ice Conditions. 9th ed.*. Can. Ice Serv., Environ, Canada, Ottawa.

Frey, K. E., Moore, G. W. K., Cooper, L. W., & Grebmeier, J. M. (2015). Divergent patterns of recent sea ice cover across the Bering, Chukchi, and Beaufort seas of the Pacific Arctic Region. *Progress in Oceanography*, *136*, 32–49. https://doi.org/10.1016/j.pocean.2015.05.009

Galley, R. J., Babb, D., Ogi, M., Else, B. G. T., Geilfus, N.-X., Crabeck, O., et al. (2016). Replacement of multiyear sea ice and changes in the open water season duration in the Beaufort Sea since 2004. *Journal of Geophysical Research: Oceans*, *121*, 1806–1823. https://doi.org/10.1002/2015JC011583

Galley, R. J., Else, B. G. T., Howell, S. E. L., Lukovich, J. V., & Barber, D. G. (2012). Landfast sea ice conditions in the Canadian. *Source: Arctic*, *65*(2), 133–144. Retrieved from. http://www.jstor.org/stable/41638586%0Ahttp://www.jstor.org/stable/

Galley, R. J., Else, B. G. T., Prinsenberg, S., Babb, D. G., & Barber, D. G. (2013). Sea ice concentration, extent, age, motion and thickness in regions of proposed offshore oil and gas development near the Mackenzie Delta-Canadian Beaufort Sea. *Arctic*, *66*(1), 105–116.

Galley, R. J., Key, E., Barber, D. G., Hwang, B. J., & Ehn, J. K. (2008). Spatial and temporal variability of sea ice in the southern Beaufort Sea and Amundsen Gulf: 1980-2004. *Journal of Geophysical Research*, *113*, C05S95. https://doi.org/10.1029/2007JC004553

Haas, C., Bublitz, A., Casey, A., & Beckers, J. (2016). Ice thickness in the Beaufort Sea and Northwest Passage in April 2016, and comparison with April 2015; Contribution to the 2016 Sea Ice Outlook coordinated by the Sea Ice Prediction Network. Retrieved from https://www.arcus.org/sipn/sea-ice-outlook/2016/informal-contributions

Haas, C., Le Goff, H., Audrain, S., Perovich, D. K., & Haapala, J. (2011). Comparison of seasonal sea-ice thickness change in the Transpolar Drift observed by local ice mass-balance observations and floe-scale EM surveys. *Annals of Glaciology*, *52*(57), 97–102. https://doi.org/10.3189/172756411795931778

Howell, S. E. L., Brady, M., Derksen, C., & Kelly, R. E. J. (2016). Recent changes in sea ice area flux through the Beaufort Sea during the summer. *Journal of Geophysical Research: Oceans*, *121*, 2659–2672. https://doi.org/10.1002/2015JC011464

Hutchings, J. K., & Rigor, I. G. (2012). Role of ice dynamics in anomalous ice conditions in the Beaufort Sea during 2006 and 2007. *Journal of Geophysical Research*, *117*, C00E04. https://doi.org/10.1029/2011JC007182

Itkin, P., & Krumpen, T. (2017). Winter sea ice export from the Laptev Sea preconditions the local summer sea ice cover and fast ice decay. *The Cryosphere*, *11*(5), 2383–2391. https://doi.org/10.5194/tc-11-2383-2017

Jackson, J. M., Carmack, E. C., McLaughlin, F. A., Allen, S. E., & Ingram, R. G. (2010). Identification, characterization, and change of the near-surface temperature maximum in the Canada Basin, 1993-2008. *Journal of Geophysical Research*, *115*, C05021. https://doi.org/10.1029/2009JC005265

Kanamitsu, M., Ebisuzaki, W., Woollen, J., Yang, S.-K., Hnilo, J. J., Fiorino, M., & Potter, G. L. (2002). NCEP-DOE AMIP-II Reanalysis (R-2). *Bulletin of the American Meteorological Society*, *83*(11), 1631–1643. https://doi.org/10.1175/BAMS-83-11-1631

Kwok, R. (2001). Deformation of the Arctic ocean sea ice cover betweenNovember 1996 and April 1997: a qualitative survey. *IUTAM Symposium onScaling Laws in Ice Mechanics and Ice Dynamics* (pp. 315–322). Dordrecht, Netherlands: Springer.

Kwok, R. (2006a). Contrasts in sea ice deformation and production in the Arctic seasonal and perennial ice zones. *Journal of Geophysical Research*, *111*, C11S22. https://doi.org/10.1029/2005JC003246

Kwok, R. (2006b). Exchange of sea ice between the Arctic Ocean and the Canadian Arctic Archipelago. *Geophysical Research Letters*, *33*, L16501. https://doi.org/10.1029/2006GL027094

Kwok, R. (2008). Summer sea ice motion from the 18 GHz channel of AMSR-E and the exchange of sea ice between the Pacific and Atlantic sectors. *Geophysical Research Letters*, *35*, L03504. https://doi.org/10.1029/2007GL032692

Kwok, R. (2015). Sea ice convergance along the Arctic coasts of Greenland and the Canadian Arctic Archipelago: Variability and extremes (1992-2014). *Geophysical Research Letters*, *42*, 7598–7605. https://doi.org/10.1002/2015GL065462

Kwok, R. (2018). Arctic sea ice thickness, volume, and multiyear ice coverage: losses and coupled variability (1958 – 2018). *Environmental Research Letters*, *13*(10), 105005. https://doi.org/10.1088/1748-9326/aae3ec

Kwok, R., & Cunningham, G. F. (2010). Contribution of melt in the Beaufort Sea to the decline in Arctic multiyear sea ice coverage: 1993-2009. *Geophysical Research Letters*, *37*, L20501. https://doi.org/10.1029/2010GL044678

Kwok, R., & Rothrock, D. A. (1999). Variability of Fram Strait ice flux and North Atlantic Oscillation. *Journal of Geophysical Research*, *104*(C3), 5177–5189. https://doi.org/10.1029/1998JC900103

Kwok, R., Spreen, G., & Pang, S. (2013). Arctic sea ice circulation and drift speed: Decadal trends and ocean currents. *Journal of Geophysical Research: Oceans*, *118*, 2408–2425. https://doi.org/10.1002/jgrc.20191

Landy, J. C., Ehn, J. K., Babb, D. G., Thériault, N., & Barber, D. G. (2017). Sea ice thickness in the Eastern Canadian Arctic: Hudson Bay Complex & Baffin Bay. *Remote Sensing of Environment*, *200*(July), 281–294. https://doi.org/10.1016/j.rse.2017.08.019

Luo, Y., & DeAbreu, R. (2010). Operational RADARSAT-2 Image Mosaicking for the Canadian Arctic Paper presented at Third RADARSAT-2 Workshop, Canadian Space Agency, St-Hubert, Que.

Lukovich, J. V., & Barber, D. G. (2006). Atmospheric controls on sea ice motion in the southern Beaufort Sea. *Journal of Geophysical Research*, *111*, D18103. https://doi.org/10.1029/2005JD006408

Maslanik, J. A., Fowler, C., Stroeve, J. C., Drobot, S., Zwally, J., Yi, D., & Emery, W. (2007). A younger, thinner Arctic ice cover: Increased potential for rapid, extensive sea-ice loss. *Geophysical Research Letters*, *34*, L24501. https://doi.org/10.1029/2007GL032043

Maslanik, J. A., Serreze, M. C., & Agnew, T. (1999). On the record reduction in 1998 Western Arctic sea-ice cover. *Geophysical Research Letters*, *26*(13), 1905–1908. https://doi.org/10.1029/1999GL900426

Maslanik, J. A., Stroeve, J. C., Fowler, C., & Emery, W. (2011). Distribution and trends in Arctic sea ice age through spring 2011. *Geophysical Research Letters*, *38*, L13502. https://doi.org/10.1029/2011GL047735

McPhee, M. G., Stanton, T. P., Morison, J. H., & Martinson, D. G. (1998). Freshening of the upper ocean in the Arctic: Is perennial sea ice disappearing? *Geophysical Research Letters*, *25*(10), 1729–1732. https://doi.org/10.1029/98GL00933

Melling, H., Riedel, D. A., & Gedalof, Z. (2005). Trends in the draft and extent of seasonal pack ice, Canadian Beaufort Sea. *Geophysical Research Letters*, *32*, L24501. https://doi.org/10.1029/2005GL024483

Moore, G. W. K., Schweiger, A., Zhang, J., & Steele, M. (2018a). Collapse of the 2017 Winter Beaufort High: A Response to Thinning Sea Ice? *Geophysical Research Letters*, *45*, 2860–2869. https://doi.org/10.1002/2017GL076446

Moore, G. W. K., Schweiger, A., Zhang, J., & Steele, M. (2018b). What Caused the Remarkable February 2018 North Greenland Polynya ? *Geophysical Research Letters*, *45*, 13,342–13,350. https://doi.org/10.1029/2018GL080902

NASA Earth Observatory (2013). Extensive Ice Fractures in the Beaufort Sea. Retrieved from https://earthobservatory.nasa.gov/images/80752

NSIDC (2013). Arctic Sea Ice News and Analysis — A fractured winter. Retrieved from http://nsidc.org/arcticseaicenews/2013/03/

NSIDC (2018a). Arctic Sea Ice News and Analysis — Arctic winter warms upto a low summer ice season. Retrieved from https://nsidc.org/arcticseaicenews/2018/05/

NSIDC (2018b). Arctic Sea Ice News and Analysis — Approaching autumn, pace slows. Retrieved from http://nsidc.org/arcticseaicenews/2018/08/approaching-autumn-pace-slows/

Nghiem, S. V., Hall, D. K., Rigor, I. G., Li, P., & Neumann, G. (2014). Effects of Mackenzie River discharge and bathymetry on sea ice in the Beaufort Sea. *Geophysical Research Letters*, *41*, 873–879. https://doi.org/10.1002/2013GL058956

Parkinson, C. L., & Comiso, J. C. (2013). On the 2012 record low Arctic sea ice cover: Combined impact of preconditioning and an August storm. *Geophysical Research Letters*, *40*, 1356–1361. https://doi.org/10.1002/grl.50349

Perovich, D. K., Richeter-Menge, J. A., Jones, K. F., & Light, B. (2008). Sunlight, water, and ice: Extreme Arctic sea ice melt during the summer of 2007. *Geophysical Research Letters*, *35*, L11501. https://doi.org/10.1029/2008GL034007

Perovich, D. K., Richter-Menge, J. A., Jones, K. F., Light, B., Elder, B. C., Polashenski, C., et al. (2011). Arctic sea-ice melt in 2008 and the role of solar heating. *Annals of Glaciology*, *52*(57), 355–359. https://doi.org/10.3189/172756411795931714

Petty, A. A., Hutchings, J. K., Richter-Menge, J. A., & Tschudi, M. A. (2016). Sea ice circulation around the Beaufort Gyre: The changing role of wind forcing and the sea ice state. *Journal of Geophysical Research: Oceans*, *121*, 3278–3296. https://doi.org/10.1002/2015JC010903

Petty, A. A., Schröder, D., Stroeve, J. C., Markus, T., Miller, J., Kurtz, N. T., et al. (2017). Skillful spring forecasts of September Arctic sea ice extent using passive microwave sea ice observations. *Earth's Future*, *5*(2), 254–263. https://doi.org/10.1002/2016EF000495

Petty, A. A., Stroeve, J. C., Holland, P. R., Boisvert, L. N., Bliss, A. C., Kimura, N., & Meier, W. N. (2018). The Arctic sea ice cover of 2016: A year of record-low highs and higher-Than-expected lows. *The Cryosphere*, *12*(2), 433–452. https://doi.org/10.5194/tc-12-433-2018

Rampal, P., Weiss, J., & Marsan, D. (2009). Positive trend in the mean speed and deformation rate of Arctic sea ice, 1979-2007. *Journal of Geophysical Research*, *114*, C05013. https://doi.org/10.1029/2008JC005066

Ricker, R., Hendricks, S., Girard-Ardhuin, F., Kaleschke, L., Lique, C., Tian-Kunze, X., et al. (2017). Satellite-observed drop of Arctic sea ice growth in winter 2015–2016. *Geophysical Research Letters*, *44*, 3236–3245. https://doi.org/10.1002/2016GL072244

Ricker, R., Hendricks, S., Kaleschke, L., Tian-Kunze, X., King, J., & Haas, C. (2017). A weekly Arctic sea-ice thickness data record from merged CryoSat-2 and SMOS satellite data. *The Cryosphere*, *11*(4), 1607–1623. https://doi.org/10.5194/tc-11-1607-2017

Rigor, I. G., & Wallace, J. M. (2002). Response of sea ice to the Arctic Oscillation. *Applied Physics*, *15*(18), 2648–2663. https://doi.org/10.1175/1520-0442(2002)015<2648:ROSITT>2.0.CO;2

Rigor, I. G., & Wallace, J. M. (2004). Variations in the age of Arctic sea-ice and summer sea-ice extent. *Geophysical Research Letters*, *31*, L09401. https://doi.org/10.1029/2004GL019492

Serreze, M. C., Crawford, A. D., Stroeve, J. C., Barrett, A. P., & Woodgate, R. A. (2016). Variability, trends, and predictability of seasonal sea ice retreat and advance in the Chukchi Sea. *Journal of Geophysical Research: Oceans*, *121*, 7308–7325. https://doi.org/10.1002/2016JC011977

Serreze, M. C., Stroeve, J. C., Barrett, A. P., & Boisvert, L. N. (2016). Summer atmospheric circulation anomalies over the Arctic Ocean and their influences on September sea ice extent: A cautionary tale. *Journal of Geophysical Research: Oceans*, *2*, 463–485. https://doi.org/10.1002/2016JD025161.Received

Simmonds, I., & Rudeva, I. (2012). The great Arctic cyclone of August 2012. *Geophysical Research Letters*, *39*, L23709. https://doi.org/10.1029/2012GL054259

Steele, M., Dickinson, S., Zhang, J., & Lindsay, R. W. (2015). Seasonal ice loss in the Beaufort Sea: Toward synchrony and prediction. *Journal of Geophysical Research: Oceans*, *120*, 1118–1132. https://doi.org/10.1002/2014JC010247

Steele, M., Zhang, J., & Ermold, W. (2010). Mechanisms of summertime upper Arctic Ocean warming and the effect on sea ice melt. *Journal of Geophysical Research*, *115*, C11004. https://doi.org/10.1029/2009JC005849

Stroeve, J. C., Maslanik, J. A., Serreze, M. C., Rigor, I. G., Meier, W., & Fowler, C. (2011). Sea ice response to an extreme negative phase of the Arctic Oscillation during winter 2009/2010. *Geophysical Research Letters*, *38*, L02502. https://doi.org/10.1029/2010GL045662

Sumata, H., Lavergne, T., Girard-Ardhuin, F., Kimura, N., Tschudi, M. A., Kauker, F., et al. (2014). An intercomparison of Arctic ice drift products to deduce uncertainty estimates. *Journal of Geophysical Research: Oceans*, *119*, 4887–4921. https://doi.org/10.1002/2013JC009724

Tilling, R. L., Ridout, A., Shepherd, A., & Wingham, D. J. (2015). Increased Arctic sea ice volume after anomalously low melting in 2013. *Nature Geoscience*, *8*(August), 643–646. https://doi.org/10.1038/NGEO2489

Timmermans, M.-L. (2015). The impact of stored solar heat on Arctic sea ice growth. *Geophysical Research Letters*, *42*, 6399–6406. https://doi.org/10.1002/2015GL064541

Tivy, A., Howell, S. E. L., Alt, B., McCourt, S., Chagnon, R., Crocker, G., et al. (2011). Trends and variability in summer sea ice cover in the Canadian Arctic based on the Canadian Ice Service Digital Archive, 1960-2008 and 1968-2008. *Journal of Geophysical Research*, *116*, C03007. https://doi.org/10.1029/2009JC005855

Tschudi, M., Fowler, C., Maslanik, J., Stewart, J. S., & Meier, W. (2016). *Polar Pathfinder Daily 25km EASE-Grid Sea Ice Motion Vectors, Version 3[1979 - 2016]* Boulder, CO: NASA National Snow and Ice Data Center Distributed Active Archive Center. https://doi.org/10.5067/O57VAIT2AYYY. [Last Accessed 8 May, 2018]

Walsh, J. E., Chapman, W. L., & Portis, D. H. (2009). Arctic cloud fraction and radiative fluxes in atmospheric reanalyses. *Journal of Climate*, *22*(9), 2316–2334. https://doi.org/10.1175/2008JCLI2213.1

Warren, S. G., Rigor, I. G., Untersteiner, N., Radionov, V. F., Bryazgin, N. N., Aleksandrov, Y. I., & Colony, R. (1999). Snow depth on Arctic sea ice. *Journal of Climate*, *12*(6), 1814–1829. https://doi.org/10.1175/1520-0442(1999)012<1814:SDOASI>2.0.CO;2

Zhang, J., Lindsay, R., Schweiger, A., & Steele, M. (2013). The impact of an intense summer cyclone on 2012 Arctic sea ice retreat. *Geophysical Research Letters*, *40*, 720–726. https://doi.org/10.1002/grl.50190